Mechanisms for restraining cAMP-dependent protein kinase revealed by subunit quantitation and novel crosslinking approaches

Ryan Walker-Gray[a], Florian Stengel[b], Matthew G. Gold[a,1]

[a]Department of Neuroscience, Physiology & Pharmacology, University College London, Gower Street, LONDON, WC1E 6BT, UK

[b]University of Konstanz, Department of Biology, Universitätsstrasse 10, 78457 Konstanz, Germany

[1]To whom correspondence may be addressed. E-mail: m.gold@ucl.ac.uk

Classification: Biological Sciences, Biochemistry

Author contributions: R.W.G., F.S. and M.G.G designed research, R.W.G., F.S. and M.G.G. performed research; and M.G.G. wrote the paper with input from R.W.G. and F.S.

The authors declare no conflict of interest.

Keywords: cAMP, Protein Kinase A, crosslinking, XL-MS, structure, anchoring

Short title: PKA subunit quantitation and crosslinking

Abstract

Protein phosphorylation by cyclic AMP-dependent protein kinase (PKA) underlies key cellular processes including sympathetic stimulation of heart cells, and potentiation of synaptic strength in neurons. Unrestrained PKA activity is pathological, and an enduring challenge is to understand how the activity of PKA catalytic subunits is directed in cells. We developed a novel light-activated crosslinking approach to monitor PKA subunit interactions with temporal precision in living cells. This enabled us to refute the recently proposed theory that PKA catalytic subunits remain tethered to regulatory subunits during cAMP elevation. Instead, we have identified other features of PKA signaling for reducing catalytic subunit diffusion and increasing re-capture rate. Comprehensive quantitative immunoblotting of protein extracts from human embryonic kidney cells and rat organs reveals that regulatory subunits are always in large molar excess of catalytic subunits (average ~17-fold). In the majority of organs tested, type II regulatory (RII) subunits were found to be the predominant PKA subunit. We also examined the architecture of PKA complexes containing RII subunits using crosslinking coupled to mass spectrometry. Quantitative comparison of crosslinking within a complex of RIIβ and Cβ, with or without the prototypical anchoring protein AKAP18α, revealed that the dimerization and docking domain of RIIβ lies between its second cAMP-binding domains. This architecture is compatible with anchored RII subunits directing the myristylated N-terminus of catalytic subunits towards the membrane for release and re-capture within the plane of the membrane.

Significance Statement

Protein phosphorylation by cyclic AMP-dependent protein kinase (PKA) triggers cellular changes including fight-or-flight responses in heart cells, and synaptic potentiation in neurons. Uncontrolled activity of PKA catalytic subunits is pathological, however the mechanism for directing PKA in cells is unclear. Using a new approach for monitoring cellular PKA subunit interactions we show that - contrary to recent proposals - catalytic subunits are released from regulatory subunits by cAMP. Instead, we identify mechanisms for rapid re-capture of liberated catalytic subunits. Regulatory subunits are expressed much more highly than catalytic subunits to support rapid catalytic subunit re-association. Furthermore, analysis of global PKA architecture reveals that type II regulatory subunit anchoring is compatible with catalytic subunit release and re-capture within the cell membrane.

\body

Introduction

cAMP-dependent protein kinase (PKA) is the major intracellular receptor for the second messenger cAMP (1). Activation of PKA by cAMP underlies responses throughout the body, including sympathetic regulation of the heart downstream of β-adrenergic receptor (β-AR) activation (2), and changes in the strength of synaptic connections between neurons (3). PKA consists of regulatory (R) subunit constitutive dimers that sequester catalytic (C) subunits prior to cAMP activation. There are two types of R subunit. Type II (RII) subunits associate with the low-speed particulate fraction after tissue homogenization, whereas RI subunits do not (4). This results from anchoring of RII, but generally not RI, at sub-cellular sites that include the cell membrane by A-kinase anchoring proteins (AKAPs) (2). Imbalances in the expression or activity of R (5) and C (6) subunits, or disruptions in PKA anchoring (7), lead to disease. An enduring challenge in cAMP/PKA research is to understand how PKA is directed to its cellular substrates. Experiments using fluorescent reporters have established that elevations in cAMP concentration and PKA activity are localized within the cell (8, 9). However, these studies do not directly address how C subunits are restrained following their release.

Following activation of an R-C complex by cAMP, the range over which the C subunit can phosphorylate substrates will depend on its rate of diffusion and the rate of re-capture by R subunits. New potential mechanisms for reducing diffusion and increasing C subunit re-capture have been investigated in recent years. N-terminal myristylation is thought to restrict some free C subunits to the intracellular face of the

membrane bilayer (10), slowing their diffusion velocity (11) and restricting their activity to the plane of the membrane. Consistent with this model, RII but not RI subunits increase binding of myristylated C subunits to liposomes (12) probably by stabilizing the 'myr-out' conformation of the myristylated C subunit A-helix (13, 14). Many AKAPs also localize to the cell and organellar membranes (15). AKAPs present amphipathic helices that bind to the dimerization and docking (D/D) domain formed by the first 45 amino acids of RII subunits (16-18). However, the first 103 amino acids of RII are not visible in the electron density of the most complete crystal structures of RII-C (13, 19) so it is not clear whether association with membrane-tethered AKAPs is compatible with inserting C subunits into the membrane.

An alternative proposed mechanism for limiting C subunit diffusion is that C subunits are never released from RII subunits but instead access nearby substrates while tethered to RII upon cAMP activation (20, 21). This theory was supported by experiments showing no effect of β-AR stimulation on C subunit co-precipitation with anchored RII subunits (20, 21). However, this experiment does not exclude the possibility that R and C subunits re-associate during co-immunoprecipitation following cell lysis. This possibility could not be excluded as, prior to our study, there has been no method to monitor association of endogenous PKA subunits in cells with temporal precision. Final aspects of PKA that could support rapid R and C subunit association are the stoichiometry and concentrations of its subunits. PKA is unusual among AGC protein kinases in that its regulatory and catalytic elements are formed by separate polypeptides (22). Binding studies show that increasing the concentration of RI subunits, with fixed C subunit concentration, increases the fraction of C subunits bound to R subunits even in

high concentrations of cAMP (23). This means that higher R subunit concentration increases the rate of R-C complex formation irrespective of cAMP concentration. Surprisingly, little information is available regarding the concentrations of endogenous PKA subunits.

We used a three-pronged approach to investigate mechanisms for restraining C subunits. This combined approach has enabled us to more clearly define which mechanisms do – and do not - contribute to restraining C subunits.

RESULTS

Light-activated crosslinking indicates that C subunits dissociate from R subunits in cells upon β-AR stimulation. To investigate the notion that C subunits remain tethered to R subunits in cells upon cAMP elevation (20, 21), we developed a novel approach that utilizes the UV light-activated crosslinker succinimidyl 4,4'-azipentanoate (SDA). We focused on human embryonic kidney (HEK) cells, which are a model cell line for studying cAMP/PKA signaling (24). An overview of this process is shown in figure 1*A*-*C*. Cells are first incubated with membrane-permeable SDA leading to covalent attachment at primary amines including lysine side-chains on RI (red, Fig. 1*A*), RII (blue) and C (green) subunits. During 365 nm illumination, the diazirine moiety of SDA may react with nearby molecules leading to covalent crosslinks (Fig. 1*B*). Since the SDA spacer arm is 3.9 Å, R-C crosslinking is strongly favoured when the two proteins are associated (Fig. 1*B*). After cell lysis, either RI subunits or RII subunits are precipitated using immobilized GST fusions (Fig. 1*C*) to the RI-selective sequence RIAD (25) or the C-terminal 93 amino acids of RII-selective AKAP79 ($AKAP79_{c93}$). R subunit precipitation is performed with cAMP so C subunit co-precipitation only occurs through R-C crosslinking. The efficacy of this approach is shown for HEK293T cells in figure 1*D*. GST alone precipitated neither RI nor RII (Fig. 1*D*, lanes 2 & 3) whereas GST-RIAD (lanes 4 & 5), and GST-$AKAP79_{c93}$ (lanes 6 & 7) respectively pulled down either RI or RII. Control experiments confirmed that GST-RIAD pulls down RIα and RIβ with similar efficiency (Fig. S1*A*, *B*). UV exposure led to co-precipitation of covalently linked

C subunits, visible as a band at 90 kD (Fig. 1*D*, IB:C) corresponding to either 1RI-1C (lane 5) or 1RII-1C (lane 7) crosslinked heterodimers.

We applied this new approach to determine if RII and C subunits remain associated upon β-AR stimulation with isoproterenol. We incubated SDA-treated HEK293T cells for five minutes with either 1 μM isoproterenol or vehicle. UV light illumination was either performed immediately, or delayed until after cell lysis. Anti-C IB signal intensity at ~ 90 kD following RII subunit pull down shows how much C subunit was bound to RII at the moment of UV illumination (indicated by arrow, Fig. 1*E*). C-RII association was reduced following isoproterenol stimulation (Fig. 1*E*, lanes 2 & 3) by 78±7% (p = 0.0015, n = 4) according to densitometry (Fig. 1*F, 'pre-lysis'*). On the other hand, C subunits were found to have returned to RII following lysis: when UV light illumination was delayed until post-lysis (Fig. 1*E*, lanes 4 & 5), isoproterenol led to a small increase in RII-C crosslinking (27±3%, p = 0.0016, n = 4, Fig. 1*F*). Re-association was abolished when we supplemented lysis buffer with 10 μM exogenous cAMP 10 min prior to UV-induced crosslinking post-lysis (Fig. S1*C*, *D*). We also performed experiments in which we coupled SDA crosslinking to GST-RIAD pull down. These experiments showed that C subunits also dissociate from RI upon isoproterenol stimulation (Fig. S1*E-F*). Together, our experiments using SDA crosslinking demonstrate that strong β-AR stimulation triggers C subunit dissociation from both RI and RII subunits in cells, and that co-precipitation of C in anti-RII immune complexes after isoproterenol stimulation (20, 21) likely occurs due to dilution of cAMP following cell lysis.

RI and RII subunits are in large excess of C subunits. The results of our SDA crosslinking experiments with live cells led us to consider alternative mechanisms for restricting C subunit activity. We next used quantitative immunoblotting to explore the possibility that R subunits outnumber C subunits. We took advantage of highly specific antibodies, which we independently validated (Fig. S2), to detect RI, C, and either the α or β isoforms of RII subunits. Our approach is exemplified for analysis of homogenates extracted from HEK293T cells (Fig. 2). HEK293T cell extract was run alongside reference concentrations of highly purified C (Fig. 2*A*, top panel), RI (second from top), RIIα (second from bottom), or RIIβ (bottom panel). Antibody binding was determined using a chemiluminescent substrate in tandem with a charge-coupled device imager, and intensity at reference subunit concentrations was used to fit Hill function calibration curves for C (Fig. 2*B*, top left panel), RI (top right), RIIα (bottom left), and RIIβ (bottom right). All protein extracts were quantified using this approach (Fig. 2*B* and Fig. S3). In the case of HEK293T cells, it was possible to approximate subunit copy numbers per cell (Fig. 2*C*, Table S1). Numbers from four independent sets of experiments revealed that there are approximately $2.42\pm0.21\times10^5$ C, $7.34\pm0.13\times10^5$ RI, $15.4\pm0.23\times10^5$ RIIα, and $3.00\pm0.69\times10^5$ RIIβ subunits per cell (Fig. 2*C*, Table S1). These copy numbers are the same order of magnitude as the GTPase Ras (26), another wide-acting signaling protein. HEK293 cell volume has been determined by different methods (27, 28) to be ~2 pL/cell. This equates to cellular PKA subunit concentrations of ~ 1.5 μM for RII, ~ 0.6 μM for RI, and ~ 0.2 μM for C subunits.

To investigate whether this uneven subunit ratio is a general feature of PKA signaling, we analyzed protein extracts collected from Sprague-Dawley rats. Brain tissue

was extracted and separated into forebrain and cerebellum, and a fraction enriched in nerve endings was also collected from forebrain. Additional extracts were prepared from heart, liver, lungs, and skeletal muscle. An identical protein extraction method was used in all cases. In sum, subunit concentrations were determined in protein extracts from eight different sample types (Fig. S3). Average concentrations (n=4) are shown in ng/mg protein extract in figure 3*A*. PKA subunit concentrations are relatively high in forebrain, with RIIβ accounting for 0.29 % total forebrain protein; and combined forebrain PKA subunits constitute 0.41 % forebrain protein (Fig. 3*A*). These concentrations are approaching those of calmodulin-dependent protein kinase II, which constitutes 0.86 % cerebral cortex (29), and calcineurin which is ~1 % of cerebral cortical and hippocampal protein (30).

We next calculated copy numbers of RI (red, Fig. 3*B*), RIIα (light blue), and RIIβ (dark blue) relative to C subunits (green) in each extract type. In all cases, R subunits greatly outnumber C subunits with a combined average of 17.2±1.7-fold more R than C subunits ($p = 4.8\text{x}10^{-6}$, Fig. 3*B*). To our knowledge, this is the first concrete demonstration of this fundamental aspect of cAMP signaling. When the average copy numbers are compared by student's t-test in each extract, both RI and RII separately outnumber C subunits with $p < 0.05$ in every case except RI in liver in which the comparison is under-powered ($p = 0.051$). R subunits are in greater than 20-fold excess of C subunits in forebrain, cerebellum and lungs. A combined analysis of all ratios reveals that RII subunits typically outnumber RI subunits by ~2:1. Cerebellum and heart are notable exceptions to this rule. The ~2-fold higher expression of RI than RII in cerebellum may be related to the different (presynaptic) role that PKA plays in synaptic

plasticity in cerebellar granule cells (31, 32). The elevated expression of the β isoform of RII in brain extracts is consistent with previous reports (33). Overall, our stoichiometric analysis reveals that C subunits are greatly outnumbered by R subunits across tissue types.

Insights into anchored type II PKA holoenzyme structure from crosslinking coupled to mass spectrometry (XL-MS). We next aimed to resolve uncertainties in the structure of anchored RII-C complexes in an effort to determine whether anchoring of RII subunits – the predominant R subunit isoform in most organs (Fig. 3*B*) – is compatible with release and capture of C subunits in the cell membrane. There are two conceivable positions for the D/D domain within the RIIβ-C complex: between the N-lobes of the C subunits, or between the second cyclic nucleotide binding (CNBB) domains of the RII subunits (13, 19). To resolve this uncertainty, we turned to XL-MS, which is a rapidly developing technique suited to structural investigation of large dynamic multi-protein complexes (34). In XL-MS, protein samples are crossslinked, digested into peptides, and the sequence of crosslinked peptides is determined by MS. Crosslinks reveal which regions of the protein complex are close in space. We utilized the homobifunctional crosslinker disuccinimidyl suberate (DSS), which links amines including those at the termini of lysine side-chains with a maximum span of ~ 30 Å (34). We first crosslinked PKA holoenzymes comprising RIIβ-Cβ, either alone or in complex with AKAP18α. AKAP18α possesses typical AKAP properties that make it a suitable prototype for studying PKA structure (18, 35) including lipid modification sites in its first six amino acids that enable membrane insertion (36). Samples were imaged using Coomassie staining, immunoblotting and RII overlay following electrophoresis either before (odd

number lanes, Fig. 4*A*) or after (even lanes, Fig. 4*A*) DSS incubation. Crosslinking of RIIβ-Cβ led to prominent bands at ~90 and 140 kD, with a weaker band at ~180 kD. Anti-C (lane 6, Fig. 4*A*), and anti-RIIβ (lane 10) immunoblots (IBs) indicate that these three species represent 2RII, 2RII-1C, and 2RII-2C. Inclusion of the AKAP shifts all three bands higher (first three panels, Fig. 4*A*) by approximately the mass of AKAP18α. RII overlay confirmed that AKAP18α was effectively crosslinked within the complex (lane 16, Fig. 4*A*). Sequences of crosslinked peptides identified in the RIIβ-Cβ and AKAP18α-RIIβ-Cβ samples are listed in Tables S2 and S3, respectively. A total of 126 crosslinked peptides were identified following crosslinking of RIIβ-Cβ, including 42 R-R intralinks, 74 C-C intralinks, and 10 R-C interlinks. Figure 4*B* shows the overall pattern of intralinks (purple), and interlinks (black) after crosslinking RIIβ (blue) and Cβ (green) in the absence of AKAP18α.

Nine different types of crosslink were identified linking RIIβ K46 at the C-terminus of the D/D domain to lysines visible in crystal structures of RIIβ-C (14, 37). In six cases, RIIβ K46 is coupled to sites in CNBB (positions 263, 266, 276, 326, 328, & 357), with a further partner lysine (Cβ K285) that projects over CNBB (Fig. 4*C*). This pattern of crosslinking is consistent with the D/D domain lying between the CNBB domains of the RIIβ dimer. XL-MS with purified RIIβ-Cβ-AKAP18α led to identification of two interlinks involving AKAP18α (Table S3): AKAP18α K19 linked to Cβ K285, and AKAP18α K65 linked to RIIβ K263. AKAP18α K19 lies between the N-terminal lipid attachment sites and the R subunit anchoring helix of the AKAP (positions 27-42), whereas K65 lies near to the C-terminus of the anchoring protein. These

interlinks are consistent with AKAP18α docking to a D/D located between the CNBB domains of the RII dimer (Fig. 4*C*). We also analyzed a complex of RIIα and Cβ using XL-MS (Fig. S4*A*, Table S4). This analysis was less powerful as the only reference lysine within the first 100 amino acids of RIIα (K71) is mid-way between the autoinhibitory sequence and D/D domain (Fig. S4*B*). Furthermore, there are no crystal structures of tetrameric RIIα-Cβ for reference. Nevertheless, the pattern of interlinks between RIIα K71 and Cβ (Fig. S4*C*) is consistent with the D/D adopting a similar position relative to the C subunit in both RII isoforms.

Quantitative XL-MS (q-XL-MS) confirms the position of the RIIβ D/D. We next quantified how addition of AKAP18α altered the abundance of crosslinks within RIIβ-Cβ. We anticipated that dynamic links would help to establish where the AKAP binds and if it alters the conformation of RIIβ-Cβ. We used the xTract algorithm (38) to identify changes in the abundance of 45 unique crosslinked sites that we were able to reliably quantify over the different replicate samples (Table S5). Five crosslinking sites decreased to less than half their original abundance upon addition of AKAP18α (Table 1, red links in Fig. 4*D*). The greatest decrease was observed for a link between RIIβ lysines 285 and 333 (5.4-fold decrease, $p = 1.32 \times 10^{-9}$, Fig. 4*D*). The four other decreasing links involved conjugation of RIIβ K46 to lysines either within (RIIβ lysines 263, 285 & 357) or adjacent to (Cβ K266) RIIβ CNBB (red, Fig. 4*D*). This pattern of down-regulated links confirms that the D/D domain of RIIβ lies between its CNBB domains: binding of AKAP18α to the D/D domain sterically impedes DSS from bridging between lysines in this region of PKA (Fig. 4*D*). Surprisingly, three crosslinks were increased by more than

50 % ($p < 0.01$) upon addition of AKAP18α (Table 1, purple, Fig. 4*E*). All three links fall within the C subunit N-lobe, suggesting that binding of AKAP18α propagates a structural rearrangement in this region that enables DSS to crosslink some N-lobe lysines more efficiently. Two of the upregulated links involve lysines within the C subunit A-helix (lysines 16 and 21, Fig. 4*E*), which is a locus for post-translational modification including myristylation. The N-terminus of AKAP18α, which is separated by ~20 amino acids from the anchoring helix, is also lipidated at three sites for insertion into the cell membrane. RII subunits, anchored to this AKAP at least, are therefore likely to orient C subunits with the myristylated A-helices pointing towards the cell membrane (Fig. 5).

DISCUSSION

This study presents three sets of experiments that clarify how PKA C subunits are controlled in cells. First, experiments using SDA demonstrate that C subunits are released from both RI and RII upon cAMP elevation, suggesting that tethering to R subunits during cAMP activation does not constitute a cellular mechanism for restricting C subunit activity. This is consistent with many *in vitro* measurements showing cAMP-induced R-C subunit dissociation using methods including scintillation proximity assay and surface plasmon resonance (23, 39), and with FRET changes between microinjected and genetically-encoded R and C subunits bearing fluorescent labels (40, 41). Second, subunit quantitation in a range of protein extracts reveals that R subunits typically exist in a ~17-fold excess of C subunits, with very high concentrations in tissues including forebrain. High subunit concentrations, and ratios heavily skewed towards R subunits, will support high rates of R-C association in cells, thereby limiting the distance from point of release over which C subunits can phosphorylate substrates. Typically, membrane-associated RII subunits outnumber RI subunits by ~2 to 1. XL-MS analysis of PKA tetramers containing RII subunits (Fig. 5 and Fig. S4) suggests that in general anchored type II isozymes orient with the N-terminus of the C subunit pointing towards the anchoring site. In the case of AKAP18α-RIIβ-Cβ, this architecture suggests that myristate (yellow, Fig. 5) and palmitate (pink) groups attached at the N-termini of AKAP18α (black) and the C subunit (green) could simultaneously insert into the cell membrane in type IIβ holoenzymes anchored to this AKAP.

We found that PKA subunit concentrations and ratios vary with tissue type (Fig. 3*B*). The four PKA R subunit isoforms are structurally and functionally different. Studies

with genetically modified mice (42) suggest that RIIβ is more functionally critical than RIIα. Type IIβ tetramers are also more compact (1) and less sensitive to cAMP (37) compared to RIIα. We found that RIIβ subunits are the predominant PKA subunit in forebrain, whereas RIIα subunits predominate in lungs and skeletal muscle (Fig. 3*B*). It should be noted that within the forebrain, RIIα and RIIβ exhibit marked neuron-specific patterns of expression (43). Genetic studies suggest that RI is more important than RII for regulating nuclear C subunit entry and concomitant gene expression (1, 23, 43). We found that RI subunits outnumber RII subunits in only heart and cerebellar extracts (Fig. 3*B*). Cardiac myxoma is a common symptom of Carney complex (CNC), which is caused in most cases by inactivation of the gene coding for RIα (5, 44). This is consistent with a prominent role for RI subunits in inhibiting cardiac C subunits. Anchored type II PKA isozymes are thought to be responsible for rapid PKA signalling processes, including ion channel regulation (15). Consistent with this model, we found very high expression levels of RII subunits in forebrain. Our XL-MS measurements show that anchoring of RIIβ, and potentially RIIα, subunits is compatible with membrane insertion of C subunits within anchored type II tetramers. Substrate concentration affects the cAMP sensitivity of type I – but not type II - PKA holoenzymes (45). The insensitivity of RII subunits to substrate concentration may support rapid C subunit binding and release within the plane of neuronal membranes where local substrate concentrations are high. Membrane tethering of C subunits released from RII subunits could potentially explain why nuclear C subunit activity is more dependent on RI subunits (23, 43). Consistent with this model, binding of C subunits to RII but not RI favours the myr-out conformation that enables efficient C subunit membrane insertion (12). A-kinase interacting protein 1 (AKIP1) and protein

kinase inhibitor peptide (PKI) will also influence the cellular localization of C subunits. AKIP1 is nuclear (46) and binds to the N-terminus of the PKA C subunit, whereas the nuclear localization of PKI is cell cycle-dependent (47). PKI could potentially inhibit ≥ 20 % C in some neurons but there is uncertainty regarding its exact concentration in brain extracts (47) so it is difficult to relate our calculated concentrations for R and C subunits to PKI.

In vitro binding studies have previously shown that the fraction of 30 nM Cα bound to RIα rises with increasing [RIα], in the presence of 50 μM cAMP, with K_d = 0.24 μM (23). Our estimates for PKA subunit concentrations in HEK293T cells (2 μM RII, 0.7 μM RI, and 0.2 μM C) show that PKA subunits are present at substantially higher concentrations than this K_d in cells. Consistent with a prediction by Kopperud and co-workers (23) that a minority of C subunits remain associated with R subunits during maximal cAMP elevation in cells, we detected residual RI-C/RII-C crosslinking upon strong β-AR stimulation at ~16/22 % of the basal crosslinking intensity according to semi-quantitative densitometry (Fig. 1*E* and Fig. S1*E*). In comparison, addition of exogenous 10 μM cAMP to post-lysis material led to a more pronounced reduction in RII-C crosslinking to ~4 % of the level without cAMP (Fig. S1*C-D*). Therefore, the residual R-C crosslinking observed in cells probably represents partial R-C association during strong β-AR stimulation of HEK293T cells. Together, our subunit quantitation and SDA measurements suggest that abundant R subunits support high rates of R-C association such that even maximal β-AR stimulation does not fully dissociate R and C subunits.

The phosphorylation state of RII subunits is also emerging as an important determinant of the rate at which C subunits bind to RII subunits (14). A recent study quantified k_{on} constants for C subunit binding to RIIα using surface plasmon resonance (14). Remarkably, dephosphorylation of RIIα Ser112 increased the k_{on} coefficient for C subunit binding by 60-fold (14). We detected molar excesses of RII subunits relative to C subunits in every rat extract tested (Fig. 3B). Therefore, typically the autoinhibitory sequences of most RII subunits will be unencumbered by C subunits and accessible to cellular phosphatases. Phosphatase access is not relevant to RI since the autoinhibition sequence of these regulatory subunits contains an alanine at the equivalent position to Ser112 (1). A recent study showed that U2OS cells expressing a fusion of RIIα and Cα subunits ('R2C2'), in place of endogenous Cα and RII subunits, exhibit PKA activity according to a cytoplasmic AKAR4 reporter following isoproterenol stimulation (21). Nuclear AKAR4 responses are blunted in cells expressing the R2C2 fusion (21). A possible explanation for these findings is that residues corresponding to the C subunit are still able to sufficiently dissociate from the regulatory elements of RII within the context of the fused R2C2 polypeptide to phosphorylate AKAR4 in the cytosol. An analogy would be activation of other AGC protein kinases by dissociation of regulatory and catalytic elements within a single polypeptide, such as in activation of protein kinase G (22). The artificially high (equimolar) ratio of C to RII, and potentially raised RII phosphorylation, in R2C2 may counterbalance reductions in cAMP-induced dissociation due to fusing the two subunits within a single polypeptide. Since the C subunit cannot diffuse away from RII after dissociation in the context of R2C2, it will be unable to pass into the nucleus, consistent with blunted nuclear AKAR4 responses in cells expressing

R2C2 (21). Nevertheless these experiments suggest that, at least in the cytosol, PKA phosphorylation can be achieved with diffusion of the C subunit over a very short distance from RII.

Rapid fluctuations in local cAMP concentration, supported by co-localization of PKA with adenylyl cyclases and phosphodiesterases, will also support faster release and binding of C subunits to R subunits. For example, type IV PDEs can anchor to AKAPs (48), and direct PKA-PDE coupling has been detected (49). XL-MS is developing rapidly, and it is plausible that the technique could be applied to study cAMP signaling complexes in cells. In future, it will be exciting to determine how anchored PKA complexes are oriented in relation to interaction partners including cyclases, phosphodiesterases and receptors (50).

Materials & Methods. For quantitative immunoblotting, samples were collected from HEK293Ts and male, four-week-old, Sprague-Dawley rats and homogenized using a DI 25 Basic rotor/stator homogenizer (Yellowline) and 20 KHz sonication. Experiments involving rats were done in accordance with the UK Animals Act, 1986, and with UCL Animal Research guidelines. For XL-MS measurements, digested PKA complexes were analyzed on Orbitrap Elite and Fusion Tribrid mass spectrometers (Thermo). For qXL-MS analysis, we compared the intensities of peaks eluting for crosslinks between the RIIβ-Cβ and RIIβ-Cβ-AKAP18α samples using xTract (38). Results are presented throughout as mean ± sem. Data were analysed by two-sided Student's t-test. *p* values are $*p<0.05$, $**p<0.01$, $***p<0.001$. Detailed methods can be found in ***SI Materials and Methods***.

Acknowledgements. We thank Annette Dolphin for use of her cell culture facility and Kanchan Chargar for assistance with cell culture. MGG is a Wellcome Trust and Royal Society Sir Henry Dale fellow (104194/Z/14/Z), and receives support from the BBSRC (BB/N015274/1). F.S. is funded by the German Science Foundation Emmy Noether Programme (STE 2517/1-1) and is grateful for support from the DFG Collaborative Research Center (SFB) 969.

References

1. Taylor SS, Ilouz R, Zhang P, & Kornev AP (2012) Assembly of allosteric macromolecular switches: lessons from PKA. *Nat Rev Mol Cell Biol* 13(10):646-658.
2. McCormick K & Baillie GS (2014) Compartmentalisation of second messenger signalling pathways. *Current opinion in genetics & development* 27:20-25.
3. Esteban JA, *et al*. (2003) PKA phosphorylation of AMPA receptor subunits controls synaptic trafficking underlying plasticity. *Nat Neurosci* 6(2):136-143.
4. Corbin JD, Sugden PH, Lincoln TM, & Keely SL (1977) Compartmentalization of adenosine 3':5'-monophosphate and adenosine 3':5'-monophosphate-dependent protein kinase in heart tissue. *J Biol Chem* 252(11):3854-3861.
5. Kirschner LS, *et al*. (2000) Mutations of the gene encoding the protein kinase A type I-alpha regulatory subunit in patients with the Carney complex. *Nat Genet* 26(1):89-92.
6. Beuschlein F, *et al*. (2014) Constitutive activation of PKA catalytic subunit in adrenal Cushing's syndrome. *N Engl J Med* 370(11):1019-1028.
7. Gold MG, Gonen T, & Scott JD (2013) Local cAMP signaling in disease at a glance. *J Cell Sci* 126(Pt 20):4537-4543.
8. Patel N & Gold MG (2015) The genetically encoded tool set for investigating cAMP: more than the sum of its parts. *Front Pharmacol* 6:164.
9. Depry C, Mehta S, Li R, & Zhang J (2015) Visualization of Compartmentalized Kinase Activity Dynamics Using Adaptable BimKARs. *Chemistry & biology* 22(11):1470-1479.

10. Gaffarogullari EC, *et al*. (2011) A myristoyl/phosphoserine switch controls cAMP-dependent protein kinase association to membranes. *Journal of molecular biology* 411(4):823-836.

11. Tillo SE, *et al*. (2017) Liberated PKA Catalytic Subunits Associate with the Membrane via Myristoylation to Preferentially Phosphorylate Membrane Substrates. *Cell reports* 19(3):617-629.

12. Gangal M, *et al*. (1999) Mobilization of the A-kinase N-myristate through an isoform-specific intermolecular switch. *Proc Natl Acad Sci U S A* 96(22):12394-12399.

13. Zhang P, *et al*. (2015) Single Turnover Autophosphorylation Cycle of the PKA RIIbeta Holoenzyme. *PLoS Biol* 13(7):e1002192.

14. Zhang P, *et al*. (2015) An Isoform-Specific Myristylation Switch Targets Type II PKA Holoenzymes to Membranes. *Structure* 23(9):1563-1572.

15. Skroblin P, Grossmann S, Schafer G, Rosenthal W, & Klussmann E (2010) Mechanisms of protein kinase A anchoring. *International review of cell and molecular biology* 283:235-330.

16. Gold MG, *et al*. (2006) Molecular basis of AKAP specificity for PKA regulatory subunits. *Mol Cell* 24(3):383-395.

17. Kinderman FS, *et al*. (2006) A dynamic mechanism for AKAP binding to RII isoforms of cAMP-dependent protein kinase. *Mol Cell* 24(3):397-408.

18. Gotz F, *et al*. (2016) AKAP18:PKA-RIIalpha structure reveals crucial anchor points for recognition of regulatory subunits of PKA. *Biochem J* 473(13):1881-1894.

19. Ilouz R, *et al*. (2012) Localization and quaternary structure of the PKA RIbeta holoenzyme. *Proc Natl Acad Sci U S A* 109(31):12443-12448.

20. Smith FD, *et al*. (2013) Intrinsic disorder within an AKAP-protein kinase A complex guides local substrate phosphorylation. *eLife* 2:e01319.

21. Smith FD, *et al*. (2017) Local protein kinase A action proceeds through intact holoenzymes. *Science* 356(6344):1288-1293.

22. Pearce LR, Komander D, & Alessi DR (2010) The nuts and bolts of AGC protein kinases. *Nat Rev Mol Cell Biol* 11(1):9-22.

23. Kopperud R, *et al*. (2002) Formation of inactive cAMP-saturated holoenzyme of cAMP-dependent protein kinase under physiological conditions. *J Biol Chem* 277(16):13443-13448.

24. Willoughby D & Cooper DMF (2007) Organization and Ca2+ regulation of adenylyl cyclases in cAMP microdomains. *Physiol Rev* 87(3):965-1010.

25. Carlson CR, *et al*. (2006) Delineation of type I protein kinase A-selective signaling events using an RI anchoring disruptor. *J Biol Chem* 281(30):21535-21545.

26. Mageean CJ, Griffiths JR, Smith DL, Clague MJ, & Prior IA (2015) Absolute Quantification of Endogenous Ras Isoform Abundance. *PLoS One* 10(11):e0142674.

27. Gillen CM & Forbush B, 3rd (1999) Functional interaction of the K-Cl cotransporter (KCC1) with the Na-K-Cl cotransporter in HEK-293 cells. *The American journal of physiology* 276(2 Pt 1):C328-336.

28. Chien HC, *et al*. (2016) Rapid Method To Determine Intracellular Drug Concentrations in Cellular Uptake Assays: Application to Metformin in Organic Cation Transporter 1-Transfected Human Embryonic Kidney 293 Cells. *Drug metabolism and disposition: the biological fate of chemicals* 44(3):356-364.

29. Erondu NE & Kennedy MB (1985) Regional distribution of type II Ca2+/calmodulin-dependent protein kinase in rat brain. *J Neurosci* 5(12):3270-3277.

30. Kuno T, *et al*. (1992) Distinct cellular expression of calcineurin A alpha and A beta in rat brain. *J Neurochem* 58(5):1643-1651.

31. Huang YY, Li XC, & Kandel ER (1994) cAMP contributes to mossy fiber LTP by initiating both a covalently mediated early phase and macromolecular synthesis-dependent late phase. *Cell* 79(1):69-79.

32. Jones BW, *et al*. (2016) Targeted deletion of AKAP7 in dentate granule cells impairs spatial discrimination. *eLife* 5:e20695.

33. Cadd G & McKnight GS (1989) Distinct patterns of cAMP-dependent protein kinase gene expression in mouse brain. *Neuron* 3(1):71-79.

34. Leitner A, Faini M, Stengel F, & Aebersold R (2016) Crosslinking and Mass Spectrometry: An Integrated Technology to Understand the Structure and Function of Molecular Machines. *Trends Biochem Sci* 41(1):20-32.

35. Tibbs VC, Gray PC, Catterall WA, & Murphy BJ (1998) AKAP15 anchors cAMP-dependent protein kinase to brain sodium channels. *J Biol Chem* 273(40):25783-25788.

36. Fraser ID, *et al*. (1998) A novel lipid-anchored A-kinase Anchoring Protein facilitates cAMP-responsive membrane events. *Embo J* 17(8):2261-2272.

37. Zhang P, *et al*. (2012) Structure and allostery of the PKA RIIbeta tetrameric holoenzyme. *Science* 335(6069):712-716.

38. Walzthoeni T, *et al*. (2015) xTract: software for characterizing conformational changes of protein complexes by quantitative cross-linking mass spectrometry. *Nat Methods* 12(12):1185-1190.

39. Herberg FW, Taylor SS, & Dostmann WR (1996) Active site mutations define the pathway for the cooperative activation of cAMP-dependent protein kinase. *Biochemistry* 35(9):2934-2942.

40. Adams SR, Harootunian AT, Buechler YJ, Taylor SS, & Tsien RY (1991) Fluorescence ratio imaging of cyclic AMP in single cells. *Nature* 349(6311):694-697.

41. Zaccolo M, *et al*. (2000) A genetically encoded, fluorescent indicator for cyclic AMP in living cells. *Nature cell biology* 2(1):25-29.

42. Kirschner LS, Yin Z, Jones GN, & Mahoney E (2009) Mouse models of altered protein kinase A signaling. *Endocrine-related cancer* 16(3):773-793.

43. Ilouz R, *et al*. (2017) Isoform-specific subcellular localization and function of protein kinase A identified by mosaic imaging of mouse brain. *eLife* 6.

44. Stratakis CA (2002) Mutations of the gene encoding the protein kinase A type I-alpha regulatory subunit (PRKAR1A) in patients with the "complex of spotty skin pigmentation, myxomas, endocrine overactivity, and schwannomas" (Carney complex). *Annals of the New York Academy of Sciences* 968:3-21.

45. Viste K, Kopperud RK, Christensen AE, & Doskeland SO (2005) Substrate enhances the sensitivity of type I protein kinase a to cAMP. *J Biol Chem* 280(14):13279-13284.

46. Sastri M, Barraclough DM, Carmichael PT, & Taylor SS (2005) A-kinase-interacting protein localizes protein kinase A in the nucleus. *Proc Natl Acad Sci U S A* 102(2):349-354.

47. Dalton GD & Dewey WL (2006) Protein kinase inhibitor peptide (PKI): a family of endogenous neuropeptides that modulate neuronal cAMP-dependent protein kinase function. *Neuropeptides* 40(1):23-34.

48. Dodge KL, *et al*. (2001) mAKAP assembles a protein kinase A/PDE4 phosphodiesterase cAMP signaling module. *Embo J* 20(8):1921-1930.

49. Krishnamurthy S, *et al*. (2014) Active site coupling in PDE:PKA complexes promotes resetting of mammalian cAMP signaling. *Biophysical journal* 107(6):1426-1440.

50. Halls ML & Cooper DM (2017) Adenylyl cyclase signalling complexes - pharmacological challenges and opportunities. *Pharmacol Ther* 170:212-225.

51. Wu J, Brown SH, von Daake S, & Taylor SS (2007) PKA type IIalpha holoenzyme reveals a combinatorial strategy for isoform diversity. *Science* 318(5848):274-279.

Figure Legends

Figure 1. Light-activated crosslinking of PKA subunits in HEK293T cells. (A) SDA covalently binds to free amine groups through its NHS moiety, including to lysines presented by RI (red), RII (blue) and C (green) subunits. (B) UV light triggers crosslinking between associated subunits. (C) Following lysis, isoform-selective R subunit pull down is performed with immobilized GST fusions. (D) R subunit pull down was performed with control GST, GST-RIAD, or GST-AKAP79$_{c93}$. R-C heterodimer precipitation (marked by arrow) required both R subunit pull-down and UV light exposure. (E) SDA-treated HEK293Ts were incubated with vehicle or 1 μM isoproterenol. Cells were then either immediately exposed to UV light ('pre-lysis'), or exposure was delayed until post lysis. RII subunits were selectively pulled down in all cases. (F) Densitometry showing that isoproterenol reduced RII-C crosslinking in live cells ('pre-lysis'). RII-C crosslinking was slightly increased by isoproterenol (n=4) when UV exposure was delayed until after lysis. ***p<0.001.

Figure 2. PKA subunit stoichiometry in HEK293T cells (A) Subunit-selective IBs for PKA subunit quantitation in HEK293T cell extract. Reference concentrations of purified Cβ, RIβ, RIIα or RIIβ were run alongside HEK293T cell extract. In the example shown, the amount of extract loaded per lane varied depending on the IB as follows (μg total protein): 32.3 (Pan C), 33.3 (Pan RI), 26.0 (RIIα), and 35.4 (RIIβ). (B) Calibration curves derived from reference protein intensities in panel A. According to the reference curves, the respective HEK293T extract lanes contained (ng subunit): 1.54 (Pan C), 4.61 (Pan RI), 12.6 (RIIα), and 2.29 (RIIβ). (C) Subunit copy numbers per HEK293T cell (n=4)

Figure 3. PKA subunit quantitation in panel of protein extracts. (A) Average subunit concentrations (n=4) are shown at ng/mg total extracted protein. Protein concentration is indicated according to the heat bar on the right. (B) Relative copy numbers of RI (red), RIIα (light blue), and RIIβ (dark blue) subunits are shown relative to C subunits (green). Numbers were determined from quantitation of extracts from four rats.*p<0.05, **p<0.01, ***p<0.001.

Figure 4. Structural insights into type IIβ PKA anchoring from XL-MS. (A) The first two lanes of each sub-panel correspond to mixtures of PKA Cβ and RIIβ; the latter two lanes correspond to AKAP18α-Cβ-RIIβ. Samples in even numbered lanes were subjected to DSS crosslinking prior to electrophoresis. The samples were visualized by Coomassie staining (5 μg sample/lane), anti-C IB (1.67 ng in lanes 5 & 7; 83 ng in lanes 6 & 8), anti-RIIβ IB (50 ng/lane), or by far-western blotting with PKA RIIα subunits (40 ng/lane). DSS crosslinking interfered with anti-C subunit antibody recognition so it was necessary to load 50-fold more material in lanes 6 & 8 than 5 & 7. (B) Distribution of intralinks (purple) and interlinks (black) within Cβ-RIIβ. Panels (C) to (E) were assembled using PDB IDs 3TNP (37) and 4ZP3 (18) with proteins colored black (AKAP18α), green (C) and blue (RIIβ) and lysine carbon-α atoms represented as spheres. (C) Location of interlinks detected between AKAP18α and Cβ –RIIβ. (D) Pattern of Cβ –RIIβ crosslinks (red) reduced by inclusion of AKAP18α. (E) Location of three intralinks (purple) within Cβ that were increased by AKAP18α addition.

Figure 5. Updated model of AKAP18α-RIIβ-Cβ complex. Proposed orientation of RIIβ (blue) dimer with associated Cβ (green) in relation to its AKAP18α (black) anchoring site and the cell membrane (grey). The location of the D/D domain, as determined from XL-MS data, suggests that myristate (yellow) and palmitate (pink) groups attached to AKAP18α and Cβ point in the same direction supporting membrane insertion of Cβ.

SUPPLEMENTARY INFORMATION for:

Mechanisms for restraining cAMP-dependent protein kinase revealed by subunit quantitation and novel crosslinking approaches

EXTENDED MATERIALS AND METHODS

Light-activated crosslinking in HEK293T cells

HEK293T cells were cultured as described in *Preparation of protein extracts*. At 80% confluence, cells were resuspended in DMEM from plates totalling 350 cm^2, and pelleted by centrifugation at 1,200 x *g* for 4 min at room temperature (RT). The cells were washed by resuspending in 10 mL PBS, and pelleted again by centrifugation for 4 min at 1,200 x *g*. 10 mM SDA (Thermo Fisher Scientific) was freshly prepared at 10 mM in DMSO. 1 mL of SDA stock was added to 9 mL PBS for a final concentration of 1 mM. This solution was used to resuspend the pelleted HEK293T cells. The cell suspension was incubated at 22 °C with 1 mM SDA on a roller mixer for 30 min, after which 1 M Tris pH 7.4 was added to a final concentration of 10 mM to quench unreacted NHS moieties. The cells were pelleted as before, the supernatant was aspirated, and the cells were washed with 10 mL PBS. The cells were next resuspended in 10 mL PBS supplemented with 1 μM isoproterenol if appropriate. Isoproterenol hydrochloride was prepared immediately prior to experiments by dissolving in PBS to produce 1 mM stock solutions. Following 5 min incubation at 22 °C, cells were next transferred to a 60 cm^2 tissue culture dish and illuminated on ice with UV light from a high-intensity Blak-Ray B-100AP 365 nm UV lamp (UVP) positioned ~ 10 cm above the surface of the plate. After illumination for 5 min, cells were pelleted as before, the supernatant was aspirated, and the cells were washed in PBS and pelleted once more. The cells were resuspended in 1 mL extraction buffer, sonicated and centrifuged at 21,100 x *g* for 1 h at 4 °C. The supernatant was collected for R subunit-selective pull down. For 'post-lysis' UV-induced crosslinking, UV-induced crosslinking was delayed until after cell lysis. In these cases, the supernatant was collected and incubated overnight at 4 °C on a rotating mixer. On the following morning, the sample was diluted into 9 mL detergent-free extraction buffer

then subjected to 5 min UV illumination as above. Post-lysis UV illumination samples were supplemented with 10 μM cAMP 10 min prior to UV illumination as appropriate.

R subunit-selective pull-down

On mornings in advance of HEK293T SDA crosslinking later in the day, 30 μL aliquots of Glutathione Sepharose 4 Fast Flow beads (GE Healthcare Life Sciences) were charged with 30 μg GST, GST-RIAD, or GST-AKAP79$_{c93}$. In each case, bead charging was performed by incubating on a rotating mixer at 4 °C for 2 h in 500 μL pull-down buffer (20 mM HEPES pH 7.5, 200 mM NaCl, 2 mM DTT, 1 mM EDTA, 0.05% TWEEN 20). The beads were washed with 4 x 1 mL pull-down buffer, then transferred to 15 mL falcon tubes in a final volume of 4.5 mL of the same buffer. 1 mL HEK293T cell extracts were divided into two, and 0.5 mL lysate was added to the appropriate charged beads (typically half to GST-RIAD, and half to GST-AKAP79$_{c93}$ beads). The mixtures were incubated overnight on a rolling mixer at 4°C. On the following morning, beads were pelleted at 1,200 x *g* for 3 min, and the supernatant was aspirated. The beads were washed with 5 x 1 mL pull-down buffer supplemented with 1 mM cAMP to remove C subunits non-covalently bound to R subunits. After the final wash step, the beads were resuspended in 1 x NuPAGE LDS Sample Buffer (Thermo Fisher Scientific) supplemented with 10 mM DTT, and incubated at 85 °C for 10 min to release GST fusion and associated proteins. Covalent attachment of C subunits to RI or RII was assessed by immunoblotting using anti-Pan C antibody. Densitometry was performed in the linear range of the antibody when performing quantitative comparisons.

To test if GST-RIAD is capable of pulling down both RIα and RIβ, 20 μL aliquots of glutathione sepharose beads, charged with 12 μg GST-RIAD, were incubated with 1 mL extraction buffer containing 0.11 ng/μL of either RIα or RIβ. After overnight incubation at 4 °C on a spinning mixer, the beads were washed with 5 x 200 μL extraction buffer, and protein was released from the glutathione sepharose as above. Pulldown efficiency was assessed by anti-Pan RI antibody IB.

Protein expression and purification

All PKA subunits purified during this investigation correspond to the human sequences. RII lysines are numbered according to the equivalent positions in crystallized mouse sequences to facilitate cross-referencing with crystal structures (2QVS for RIIα, 3TNP for RIIβ). PKA Cβ, RIα, RIβ, RIIα, RIIβ, AKAP18α, AKAP79 (335-427), and RIAD were expressed as PreScission-cleavable fusions at the C-terminus of GST using the vector pGEX6P1. PKA Cα was expressed with an N-terminal 6xHis tag using pET28a. All proteins were expressed in *E. coli* BL21 (DE3) cells by inducing cultures of 1.6-4.8 L at an OD_{600nm} ~ 0.7 with 375 μM IPTG. Following incubation with shaking at 20 °C overnight, cells were pelleted by centrifugation for 10 min at 4,000 x *g*. Cell pellets were washed in PBS, and frozen at -80°C prior to processing. All protein purification steps were performed on ice. For cell lysis, cell pellets were thawed in 50-100 mL of either glutathione sepharose binding buffer (30 mM HEPES pH 7.5, 500 mM NaCl, 2 mM DTT, 0.5 mM EDTA, and 1 mM benzamidine) or Ni-NTA binding buffer (30 mM Tris pH 8.0, 500 mM NaCl, 10 mM Imidazole, 1 mM benzamidine) as appropriate. All lysates were supplemented with 0.1 μg/mL lysozyme; lysates for purifying AKAP18α, Cβ, RIIβ, RIα were supplemented with 10 % glycerol; the AKAP18α lysate was supplemented with 0.5 % Triton TX-100; and the Cα lysate was supplemented with one Complete EDTA-free protease inhibitor tablet (Roche) per 100 mL lysate. Lysates were sonicated at 20 kHz for 2 x 30 s then mixed on a roller for 30 min prior to centrifucation at 31,360 x *g* for 30 min. Clarified supernatants were incubated for either 3 h with 2 mL Glutathione Sepharose 4B (GE Healthcare Life Sciences) or 1 h with 2 mL Ni-NTA agarose (Qiagen) as appropriate. Following binding, affinity beads were washed with 3 x 10 mL binding buffer prior to elution.

Elution from glutathione sepharose was performed in two ways depending on whether cleavage from GST was desired. For GST fusion proteins, elution was performed by incubating for 1 h with 2 mL of binding buffer supplemented with 10 mM L-glutathione. For release of purified PKA subunit alone, beads were incubated with 60 μg PreScission protease (GE Healthcare Life Sciences) in 2 mL glutathione sepharose binding buffer. In this case, elution was performed by overnight incubation at 4°C. Elution of His-tagged Cα subunits from Ni-NTA agarose was performed in batch by

incubating with Ni-NTA elution buffer (30 mM Tris pH 7.0, 500 mM NaCl, 300 mM imidazole, 1 mM benzamidine). In the final purification step, all protein samples were separated by size exclusion chromatography (SEC) using an 80 mL Superdex 200 column (GE Healthcare Life Sciences) controlled by an ÄKTA fast protein liquid chromatography system (GE Healthcare Life Sciences). SEC was performed with HEPES-NaCl buffer (20 mM HEPES pH 7.5, 200 mM NaCl). High purity protein was collected from peak fractions on the basis of Coomassie staining fractions separated by gel electrophoresis on 4-12 % Bis-Tris NuPAGE gels (Thermo Fisher Scientific).

Preparation of protein extracts

Male, four-week-old, Sprague-Dawley rats were euthanized by cervical dislocation, and organs were removed immediately. Forebrain, cerebellum, heart, tibialis anterior muscle, lung, and liver were excized on ice, washed in phosphate-buffered saline (PBS), and weighed. Extraction buffer (30 mM HEPES pH 7.5, 150 mM NaCl, 0.5 mM EDTA, 1 mM benzamidine, 1% (w/v) Igepal CA-630, and 0.25% (w/v) sodium deoxycholate) was added to each sample at 1 mL per 100 mg wet mass. The organs were manually sliced into smaller pieces before homogenization at 9,500 rpm using a Di 25 basic rotor/stator homogenizer (Yellowline) for 2 x 30 s. The homogenate was next sonicated for 30 s at 20 KHz and finally clarified by centrifugation at 21,130 x *g* for 1 h at 4 °C. The resulting supernatant was collected for quantitative immunoblotting and measurement of total protein content using bicinchoninic acid (BCA) assay. The concentration of protein in extracts was determined by BCA assay (mg/mL): cerebellum (6.68±0.70), forebrain (8.52±0.25), heart (7.73±0.71), liver (13.50±1.38), lung (8.21±1.15), skeletal muscle (5.71±0.48), and nerve-ending rich forebrain fraction (8.83±0.48). Nerve ending-enriched fractions were collected using Dounce homogenization to fraction 'S1'. Briefly, rat forebrains were excized, rinsed in ice cold sucrose/EDTA buffer (0.32 M sucrose, 1 mM EDTA, 5 mM HEPES pH 7.4), weighed, and resuspended in 3.5 mL sucrose/EDTA buffer. After coarse manual chopping, the sample was processed using a Dounce homogenizer (5 strokes with loose insert followed by 5 strokes with tight insert). The homogenate was centrifuged at 1,000 x *g* for 10 min, and the resulting supernatant was

collected for analysis. BCA assay indicated that this protocol yields ~ 30 mg protein per g starting wet mass.

In advance of preparation of protein extracts, HEK293T cells were cultured in Dulbecco's modified eagle media (DMEM) supplemented with 100 units/mL penicillin, 100 μg/mL streptomycin, 10 % fetal bovine serum, and 2 mM glutaMAX at 37°C in 5% CO_2. All tissue culture media and additives were supplied by Gibco. Cells at ~ 70 % confluence on T75 plates were washed and resuspended in PBS, and cell number/mL was determined using a haemocytometer to enable the average number of cells per μg total protein extract to be calculated later in the analysis. Next, the cells were pelleted at 1,200 x *g*, resuspended in 700 μL extraction buffer, and sonicated for 30 s at 20 MHz. The lysate was clarified by centrifugation for 1 h at 21,130 x *g*. The supernatant was collected for immunoblotting and analysis/BCA assay.

Quantitative immunoblotting

Immunoblotting was performed using mouse anti-PKA subunit primary antibodies purchased from BD Biosciences. Antibodies were diluted to 0.8 μg/mL in Tris-buffered saline + 0.05 % Tween-20 (TBS-T) supplemented with 10 % milk (w/v) with the exception of pan-C antibody (0.5 μg/mL). Experiments were performed using antibodies recognizing C subunits (detection range 0.1-100 ng, product number 610981), RI subunits (1-100 ng, 610166), RIα (n/a, 610609), RIIα (3-50 ng, 612243), and RIIβ (3-50 ng, 610626). Primary antibodies were coupled to goat anti-mouse IgG (H+L) poly-horseradish peroxidase (HRP) secondary antibody (Thermo Fisher Scientific), and peroxidase was detected with SuperSignal™ West Dura substrate (Thermo Fisher Scientific) using an ImageQuant imaging unit (GE Healthcare Life Sciences). Band intensities for reference protein standards and experimental samples were calculated using ImageJ (NIH) for background subtraction and pixel integration. For each IB, reference curves were established by fitting to Hill functions using iterative least-squares refinement with the Levenberg-Marquardt algorithm in ORIGIN software (OriginLab). Fitted curves (with typical R^2 coefficients > 0.99) were used to determine the protein concentration of the given PKA subunit in experimental samples transferred on the same nitrocellulose membrane. Calibration experiments were performed to determine optimal

sample loading volumes and exposure times that generated signal within the dynamic range of the relevant antibody before the full analysis (n=4 for each subunit in each extract) was completed.

PKA subunit copy numbers per HEK293T cell (**Fig. 2C** & **Table S1**) were calculated according to the following formula:

$$\text{Subunit number (cell}^{-1}\text{)} = \left(\frac{\text{Subunit/total protein (g/g)}}{\text{Subunit MW (gmol}^{-1}\text{)}}\right) * \text{Avogradro's constant (mol}^{-1}\text{)} * \text{Total protein extracted per cell (gcell}^{-1}\text{)}$$

Crosslinking coupled to mass spectrometry (XL-MS)

RIIα-Cβ, RIIβ-Cβ, and RIIβ-Cβ-AKAP18α complexes were crosslinked in 100 µL HEPES-NaCl buffer comprising 50 µg RIIα + 50 µg Cβ, 50 µg RIIβ + 50 µg Cβ, and 50 µg RIIβ + 50 µg Cβ + 5 µg AKAP18α, respectively. The samples were pre-incubated at 30°C for 10 min shaking at 500 rpm in a Thermomixer (Eppendorf). Crosslinking was initiated by addition of 0.5 mM H12/D12 DSS (Creative Molecules) from a 25 mM stock prepared in DMSO. After a further 30 min shaking at 30 °C, crosslinking was quenched by addition of 50 mM ammonium bicarbonate from a 1 M stock. During analysis of electrophoretically-separated crosslinked samples, AKAP18α was detected by far-western blotting with V5-tagged RIIα subunits coupled to anti-V5-HRP antibody (Thermo Fisher Scientific). Prior to analysis on the mass spectrometer, crosslinked samples were treated with a urea/tris(2-carboxyethyl)phosphine (TCEP) solution to reduce disulphide bonds, after which free cysteines were alkylated with iodoacetimide. Protein was next digested with trypsin, and the resulting trypsinized peptide mixture was treated with formic acid to inhibit trypsin activity. Digested peptides were separated from the solution and retained by a solid phase extraction system, and then separated by SEC prior to liquid chromatography (LC)-MS/MS analysis on Thermo Scientific Orbitrap Elite (RIIβ-containing samples) or Orbitrap Fusion Tribrid (RIIα-containing samples) mass spectrometers. Data were searched using *xQuest* in ion-tag mode with a precursor mass tolerance of 10 ppm. For matching of fragment ions, tolerances of 0.2 Da for common-ions and 0.3 Da for cross-link ions were applied. Crosslinked samples were

prepared in duplicate for all complexes, and each of these was measured with technical duplicates. Crosslinks were only considered during structural analysis if they registered ID scores >20 and deltaS < 0.95.

Quantitative crosslinking coupled to mass spectrometry (*q*XL-MS)

For *q*XL-MS analysis, we compared the intensities of peaks eluting for crosslinks between the RIIβ-Cβ and RIIβ-Cβ-AKAP18α samples (n=2, each sample analysed in duplicate). Amounts of potential crosslinks were normalized prior to MS by measuring peptide bond absorption at 215 nm for each fraction. Only high-confidence crosslinks that were identified in all biological experiments were selected for further quantitative analysis. Quantities of identified high-quality crosslinks were determined by xTract (37).

Statistical analysis

Results are presented throughout as mean ± sem. Data were analyzed by two-sided Student's t-test. *P* values are $*P<0.05$, $**P<0.01$, $***P<0.001$.

SUPPLEMENTARY FIGURE & TABLE LEGENDS

Figure S1. Supporting experiments for UV-induced crosslinking of PKA subunits in HEK293T cells (A) We tested if GST-RIAD is capable of pulling down both RIα and RIβ. Magnetic glutathione sepharose beads were charged with GST-RIAD and incubated with extraction buffer containing 0.11 ng/μL RIα or RIβ. The beads were washed, protein was eluted with SDS loading buffer, and RI precipitation was compared by anti-RI IB. (B) Relative to the input material, according to densitometry, RIα was enriched by 14.3±1.8-fold (n=3), and RIβ by 15.1±0.6-fold (n=4). This experiment indicates that GST-RIAD pulls down both RI isoforms with similar efficiency. (C & D) Effect of isoproterenol treatment and timing of UV exposure on RI-C crosslinking in HEK293T cells. (C) Control experiment to test whether addition of cAMP prevents RII-C crosslinking when crosslinking is performed by UV illumination 'post-lysis' following isoproterenol stimulation. 10 μM cAMP was added 10 min before UV illumination for the + cAMP condition (lane 3). RII-C crosslinking was assessed by anti-RII IB following pull-down with GST-AKAP79$_{c93}$. (D) Whereas the crosslinked RII-C band was 2.15±0.08 times as intense as the input C subunit band according to anti-C IB, addition of cAMP reduced RII-C signal to only 0.04±0.01 as much as the input C subunit. This indicates that addition of cAMP during post-lysis UV-induced crosslinking reduces RII-C crosslinking by ~ 50-fold (p=0.0014, n=3). (E) Cells were incubated first with SDA, then in PBS either with or without 1 μM isoproterenol. After 5 min, the cells were either exposed to UV light immediately ('pre-lysis', lanes 3 & 4), or UV illumination was delayed until after cell lysis ('post lysis', lanes 4 & 5). RI subunits were selectively precipitated using GST-RIAD attached to glutathione magnetic beads in all cases. RI-C subunit association at the moment of UV illumination was revealed by the intensity of the band at ~ 90 kD in the anti-C subunit IB as indicated by the arrow. (F) Densitometry confirmed that isoproterenol led to reduced RI-C crosslinking both in live cells ('pre-lysis', -84±3%, n=4, p = 1.18 x 10^{-4}), and when UV exposure was delayed until after cell lysis ('post-lysis', - 63±5%, n=4, p = 9.03 x 10^{-4}). C subunits can bind RII but not RI subunits in the absence of Mg^{2+} and ATP (38). In addition, RI holoenzymes are more sensitive to cAMP than RIIβ holoenzymes (1). These differences may explain why C

subunits do not re-associate with RI as efficiently as RII (Fig. 2*E*) upon cell lysis following isoproterenol stimulation.

Figure S2. Anti-PKA subunit antibody validation. In advance of quantitative immunoblotting experiments with proteins extracts from rat organ and HEK293T cells, we assessed the specificity of anti-PKA subunit antibodies sold by BD Biosciences. For each antibody, binding was tested to a panel of highly purified human PKA subunits. The purity of each subunit used for antibody validation is demonstrated by Coomassie staining (A). In panels (B) to (F) the catalog number for BD Biosciences, and the amount of PKA subunit loaded in each lane is listed. (B) Pan-C antibody recognized both Cα and Cβ with equal efficiency (lanes 1 & 2). This antibody was raised against purified human PKA C subunit α isoform residues 18-347. This region is 94% identical to the equivalent region in the β isoform. The antibody is highly sensitive and also proved to be useful for light-activated crosslinking experiments. (C) Pan-RI antibody bound equally well to RIα and RIβ as expected. This antibody was raised against residues 285-351 of RIα, which have 88% identity with the equivalent region of RIβ. On the other hand, antibody marketed as being selective for the α isoform of RI (D) also bound to RIβ (lane 4) albeit with some preference for RIα (2.3-fold higher signal, D). We therefore did not attempt to distinguish relative levels of RIα and RIβ in quantitative IBs. RIIα (E, lane 5) and RIIβ (F, lane 6)-specific antibodies showed no cross-reactivity. We therefore proceeded with Pan-C, Pan-RI and RII isoform-specific antibodies for determination of PKA subunit stoichiometries.

Figure S3. PKA subunit quantitation in rat extracts. Panels A to D show example quantitative IBs for determination of PKA subunit concentrations per total protein extracted in eight different extract types. In each panel, IBs are shown on the left-hand side, and the position of band intensities on reference curves derived from the reference protein series are shown on the right (A) Anti-C subunit IB. The reference protein is purified Cβ. The following amounts of total extracted protein were loaded (μg): 32.3 (HEK293T), 13.8 (nerve ending-rich), 11.2 (forebrain), 31.1 (cerebellum), 25.8 (heart), 101 (liver), 61.4 (lungs), and 47.9 (skeletal muscle). (B) Anti-RI IB. The reference

protein is purified RIβ. The following amounts of total extracted protein were loaded (μg): 33.3 (HEK293T), 113 (liver), 50.6 (lung), 60.4 (skeletal muscle), 12.3 (nerve ending-rich), 17.0 (forebrain), 10.5 (cerebellum), 21.0 (heart). (C) Anti-RIIα IBs. The reference protein is purified RIIα. The following amounts of total extracted protein were loaded (μg): 26.0 (HEK293T), 47.3 (nerve ending-rich), 28.5 (forebrain), 31.1 (cerebellum), 79.9 (heart), 101 (liver), 41.4 (lungs), and 39.7 (skeletal muscle). (D) Anti-RIIβ IBs. The reference protein is purified RIIβ. The following amounts of total extracted protein were loaded (μg): 31.8 (nerve ending-rich), 22.3 (forebrain), 24.9 (cerebellum), 79.9 (heart), 52.8 (lung), 39.8 (HEK293T), 57.0 (skeletal muscle), 189 (liver). In all cases, final average subunit concentrations were determined from the average of four replicates.

Figure S4. **Structural insights into type IIα PKA anchoring from XL-MS** (A) Each sub-panel corresponds to Cβ-RIIα subunits before (lanes 1, 3 & 5) and after (2, 4 & 6) DSS crosslinking. The samples were visualized by Coomassie staining (5 μg sample/lane, lanes 1 & 2), anti-C IB (25 ng in lane 3; 100 ng in lane 4), and anti-RIIβ IB (12.5 ng/lane, lanes 5 & 6). DSS crosslinking interfered with anti-C subunit antibody recognition so it was necessary to load more material in lane 4 than 3. (B) Distribution of intralinks (grey) and interlinks (black) within Cβ-RIIα. Panel (C) was assembled using PDB ID 2QVS (8), and shows the positions of four lysines (Cα atoms as black spheres) in Cβ that were detected in interlinks paired to RIIα K71. The surface of RIIα is shown in blue, with Cβ in green. Cβ lysines that were not detected in interlinks to RIIα K71 are shown as green spheres. The first visible amino acid in the RIIα – Cβ heterodimer crystal structure (8) is T91. RIIα K71 (the only lysine within the first 100 amino acids of RIIα) lies midway between T91 and the RIIα D/D domain (second helix ends at ~ position 43) so links involving this lysine provide information of the path of the linker between the autoinhibitory site and D/D domain. Four interlinks were detected between RIIα K71 and sites in Cβ, with all four sites falling in the C-lobe of the catalytic domain. RIIα K71 interlinked strongly to a triad of lysines at the base of the Cβ C-lobe: multiple interlinks were detected for lysines 254, 266 & 279 (shown in black). A further interlink was detected between RIIα K71 and Cβ K317. This pattern of interlinking is consistent with

the linker prior to the autoinhibitory site taking a path to the base of the C-lobe. This could potentially position the RIIα D/D domain in a similar orientation with respect to the C subunit as in the RIIβ holoenzyme (**Fig. 4C & D**). In comparison to RIIβ-Cβ XL-MS, there are reasons for caution in interpreting the results of RIIα-Cβ crosslinking. Whereas, RIIβ K46 lies at the immediate C-terminus of the D/D domain, the key reference K71 in RIIα is mid-way between the D/D domain and autoinhibitory site. Furthermore, the pattern of intralinks within RIIα involving RIIα K71 is difficult to interpret (**Fig. S4B, Table S4**) as there is no reference tetrameric reference crystal structure for RIIα-Cβ unlike RIIβ-Cβ (51).

Table S1. Calculation of PKA subunit copy numbers per HEK293T cell. Copy numbers were determined according to the formula listed under the heading "Quantitative immunoblotting" in Supplemental Information. *The MW of Cα was used, since this is the predominant isoform in HEK293T cells according to the molecular weight detected with pan-C antibody (e.g., Fig 1*D*). **Average of RIα (42,982 Da) and RIβ (43,073 Da).

Table S2. XL-MS data following RIIβ-Cβ DSS crosslinking. The first column lists the amino acid sequence of crosslinked peptides and the positions of the crosslinked lysine residues. “deltaS” is a measure for how close the best assigned hit was scored in regard to the second best. The peptides are listed in order of “ID-Score”, which is a weighted sum of different used to assess the quality of the composite MS2 spectrum as calculated by *xQuest*.

Table S3. XL-MS data following RIIβ-Cβ-AKAP18α DSS crosslinking. Column labels are the same as described in the legend to Table S2.

Table S4. XL-MS data following RIIα-Cβ DSS crosslinking. Column labels are the same as described in the legend to Table S2.

Table S5. Quantitative XL-MS comparison of crosslinking site intensity ± AKAP18α. The table lists the relative change in crosslinking between different lysine pairs within RIIβ-Cβ upon inclusion of AKAP18α**.** Lysine pairs are listed starting with the link that was most reduced by inclusion of AKAP18α. Changes in abundance are expressed as $\log_2$ (abundance with AKAP18α/abundance without AKAP18α). *p* value indicates the regression between the two conditions.

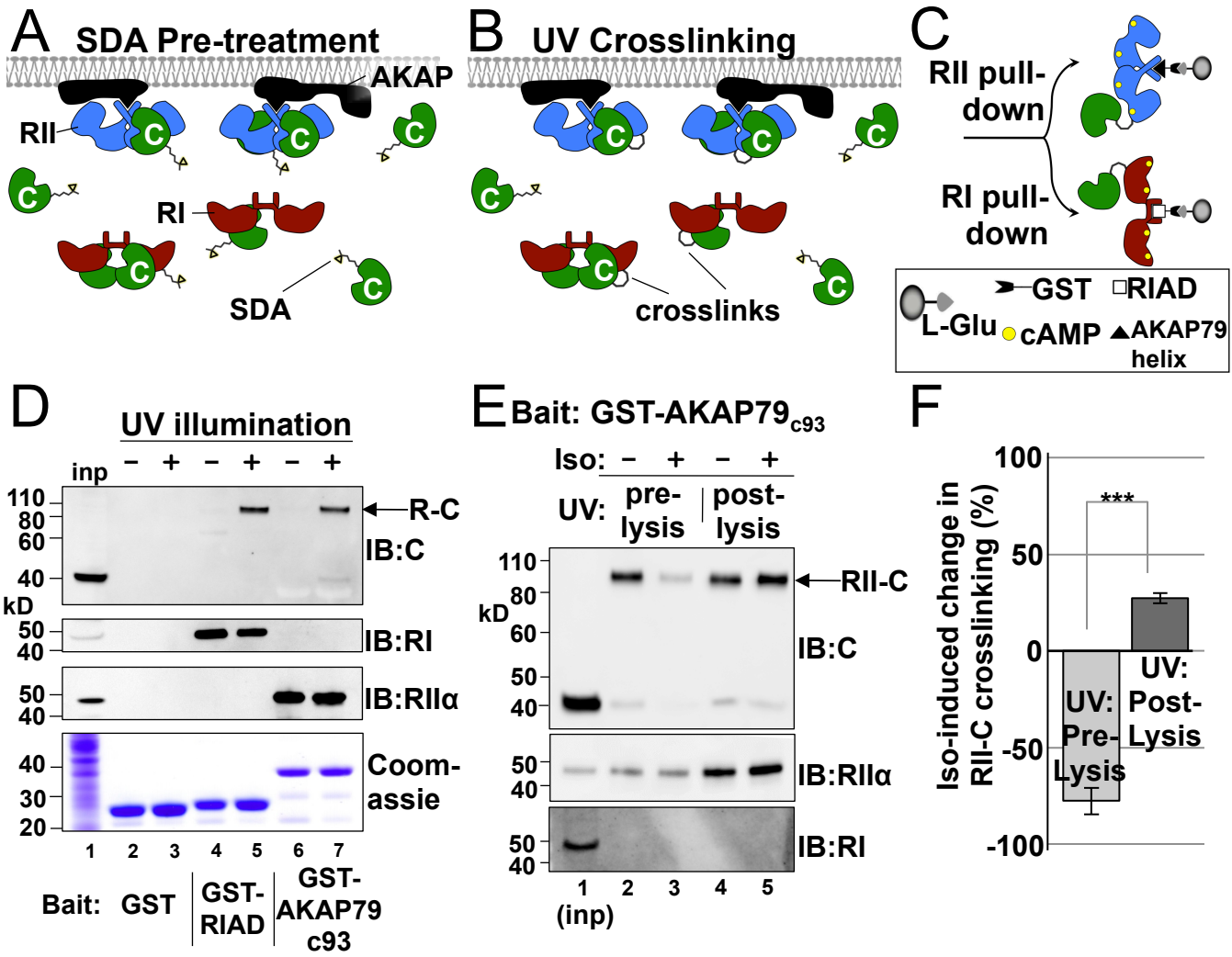
A
SDA Pre-treatment
AKAP
RII
C
RI
SDA
B
UV Crosslinking
crosslinks
C
RII pull-down
RI pull-down
GST
RIAD
L-Glu
cAMP
AKAP79 helix
D
UV illumination
inp
− + − + − +
110
80
60
40
kD
R-C
IB:C
50
40
IB:RI
IB:RIIα
Coom-assie
30
20
1 2 3 4 5 6 7
Bait: GST
GST-RIAD
GST-AKAP79 c93
E
Bait: GST-AKAP79c93
Iso: − + − +
UV: pre-lysis | post-lysis
RII-C
1 2 3 4 5
(inp)
F
Iso-induced change in RII-C crosslinking (%)
100
50
0
-50
-100
***
UV: Pre-Lysis
UV: Post-Lysis

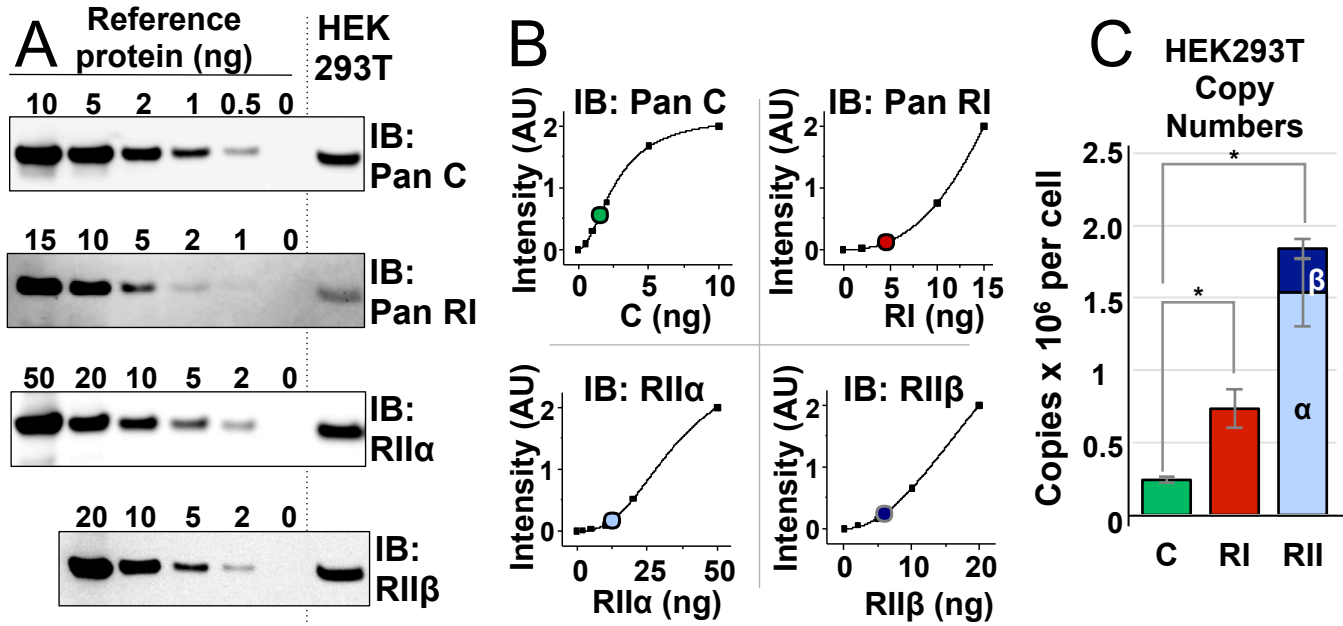
A
Reference protein (ng)
HEK 293T
10 5 2 1 0.5 0
IB: Pan C
15 10 5 2 1 0
IB: Pan RI
50 20 10 5 2 0
IB: RIIα
20 10 5 2 0
IB: RIIβ
B
IB: Pan C
Intensity (AU)
C (ng)
IB: Pan RI
RI (ng)
IB: RIIα
RIIα (ng)
IB: RIIβ
RIIβ (ng)
C
HEK293T Copy Numbers
Copies x 10^6 per cell
β
α
C
RI
RII

A

	HEK 293T	N.E.-Rich	Fore-brain	Cere-bellum	Heart	Liver	Lungs	Skeletal muscle
C	56.6 ± 4.0	147 ± 34	184 ± 37	62.2 ±6.3	126 ± 16	11.7 ± 1.2	32.3 ± 3.8	50.6 ± 7.1
RI	183 ± 34	962 ± 137	608 ± 60	1,050 ± 150	528 ± 82	60.7 ± 11	118 ± 14	97.3 ± 17.9
RIIα	409 ± 72	238 ± 36	396 ± 61	346 ± 37	223 ± 41	84.6 ± 13.9	420 ± 56	414 ± 48
RIIβ	82.9 ± 23.1	2,400 ± 180	2,870 ± 340	247 ± 50	52.5 ± 5.6	24.1 ± 2.9	223 ± 30	82.8 ± 8.8

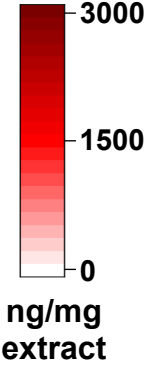

B

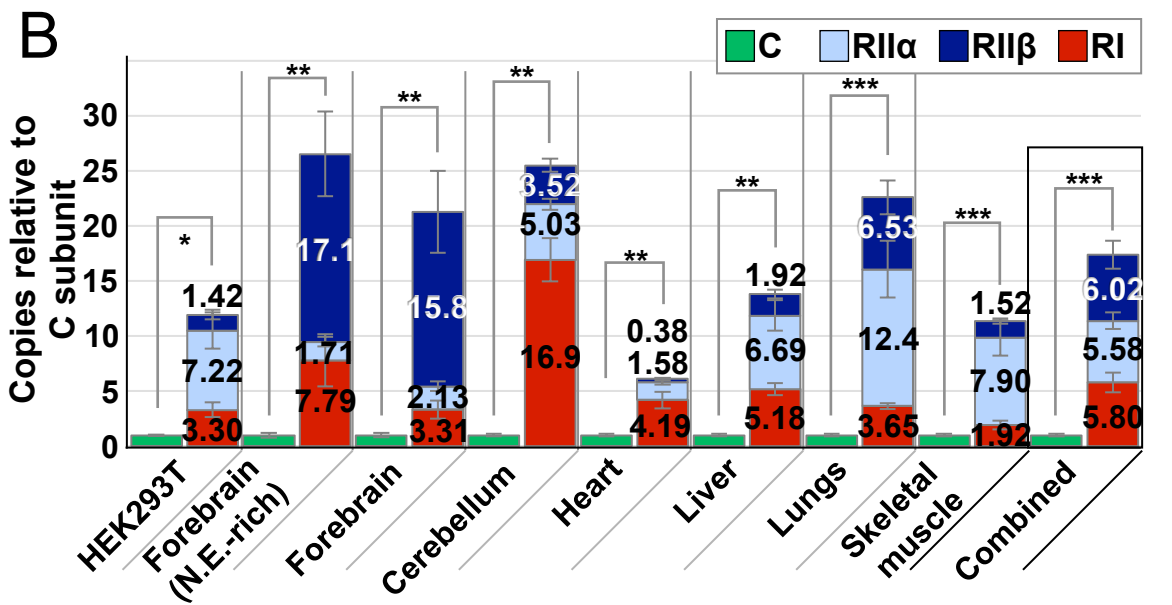

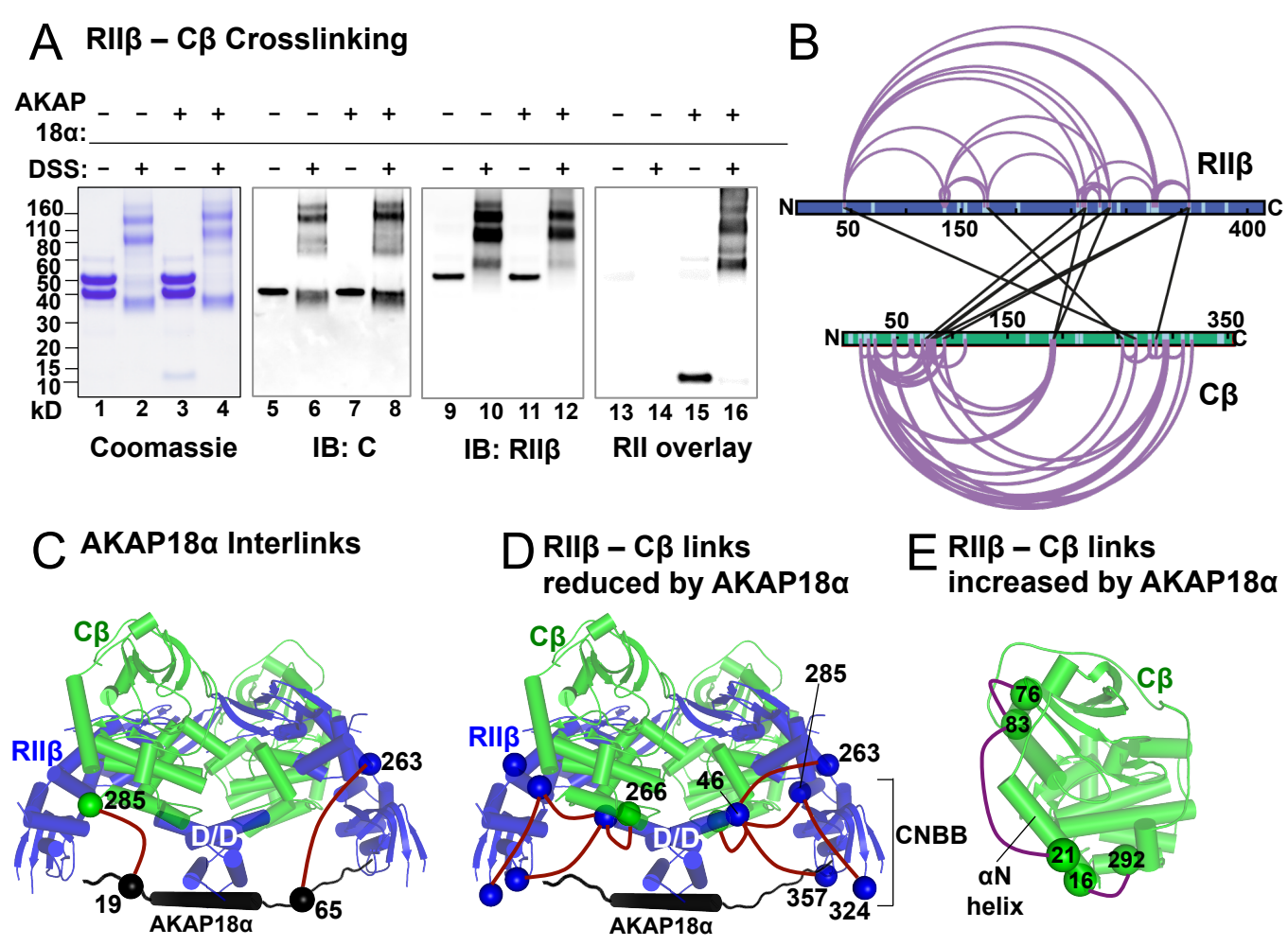
A
RIIβ – Cβ Crosslinking
AKAP
18α:
DSS:
160
110
80
60
50
40
30
20
15
10
kD
1 2 3 4
5 6 7 8
9 10 11 12
13 14 15 16
Coomassie
IB: C
IB: RIIβ
RII overlay
B
RIIβ
N
C
50
150
400
50
150
350
N
C
Cβ
C
AKAP18α Interlinks
Cβ
RIIβ
263
285
D/D
19
AKAP18α
65
D
RIIβ – Cβ links
reduced by AKAP18α
Cβ
285
RIIβ
263
266
46
D/D
CNBB
357
324
AKAP18α
E
RIIβ – Cβ links
increased by AKAP18α
Cβ
76
83
21
292
16
αN
helix

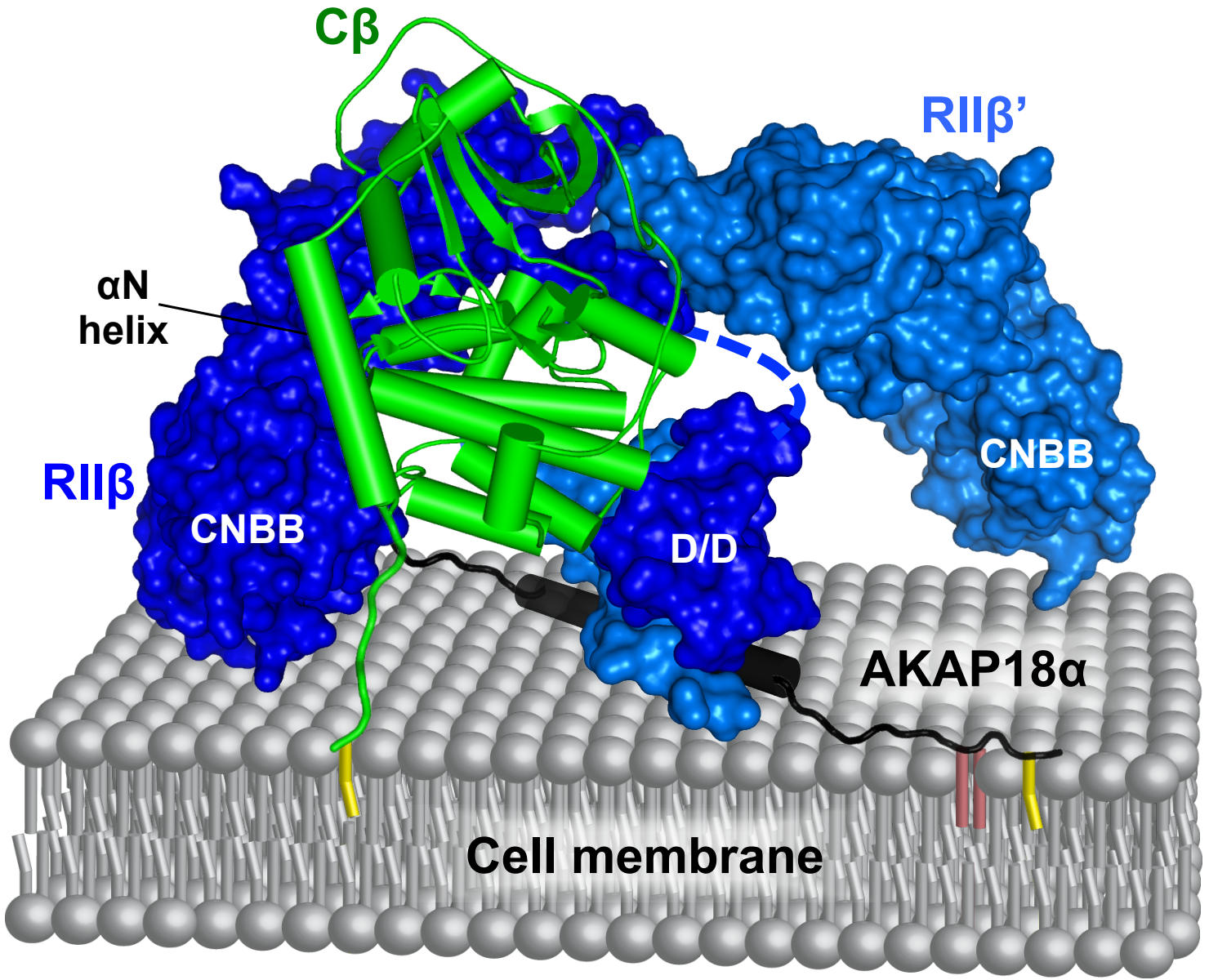
Cβ
RIIβ'
αN
helix
RIIβ
CNBB
CNBB
D/D
AKAP18α
Cell membrane

Table 1. Crosslinks in RIIβ-Cβ affected by addition of AKAP18α. Unique crosslinking sites are listed whose abundance either increased by more than 50 %, or decreased to less than 50 % upon addition of AKAP18α. $p < 0.01$ for all sites. Data for all 45 unique crosslinking sites that could be reliably quantified are listed in Table S5.

Dynamic Crosslink	Ratio (+/-AKAP18α)	*p* value
Decreased abundance + AKAP18α		
RIIβ K285 - RIIβ K324	0.186	1.32×10^{-9}
Cβ K266 - RIIβ K46	0.345	2.58×10^{-3}
RIIβ K263 - RIIβ K46	0.387	1.58×10^{-5}
RIIβ K285 - RIIβ K46	0.424	1.3×10^{-6}
RIIβ K357 - RIIβ K46	0.462	1.17×10^{-4}
Increased abundance + AKAP18α		
Cβ 16 - Cβ 292	2.12	1.26×10^{-6}
Cβ 21 - Cβ 83	1.92	2.23×10^{-4}
Cβ 76 - Cβ 83	1.64	4.07×10^{-6}

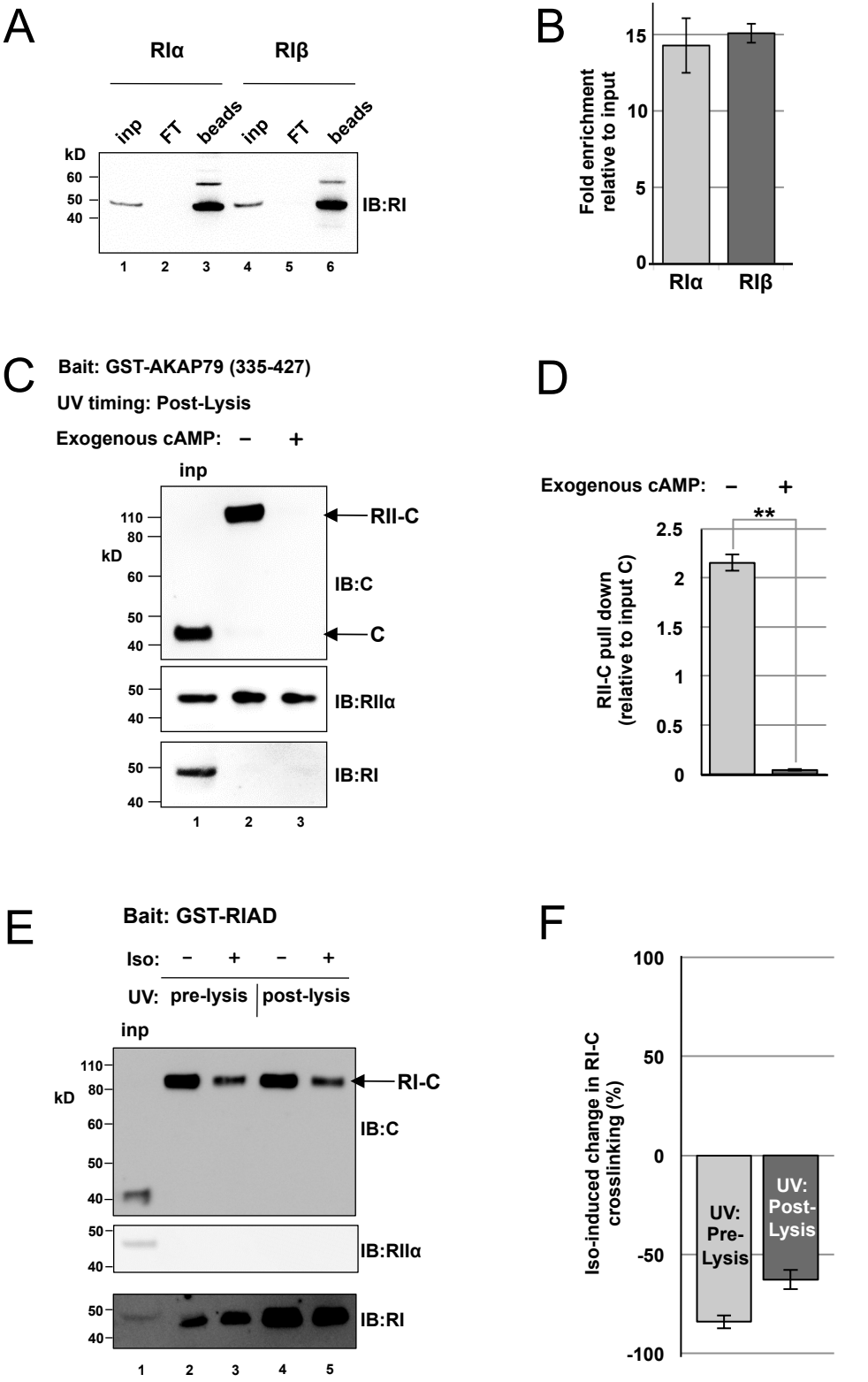
A
RIα
RIβ
inp
FT
beads
inp
FT
beads
kD
60
50
40
IB:RI
1 2 3 4 5 6
B
Fold enrichment relative to input
15
10
5
0
RIα
RIβ
C
Bait: GST-AKAP79 (335-427)
UV timing: Post-Lysis
Exogenous cAMP: – +
inp
110
80
kD
60
50
40
RII-C
IB:C
C
50
40
IB:RIIα
50
40
IB:RI
1 2 3
D
Exogenous cAMP: – +
**
RII-C pull down (relative to input C)
2.5
2
1.5
1
0.5
0
E
Bait: GST-RIAD
Iso: – + – +
UV: pre-lysis | post-lysis
inp
110
80
kD
60
50
40
RI-C
IB:C
50
40
IB:RIIα
50
40
IB:RI
1 2 3 4 5
F
Iso-induced change in RI-C crosslinking (%)
100
50
0
-50
-100
UV: Pre-Lysis
UV: Post-Lysis

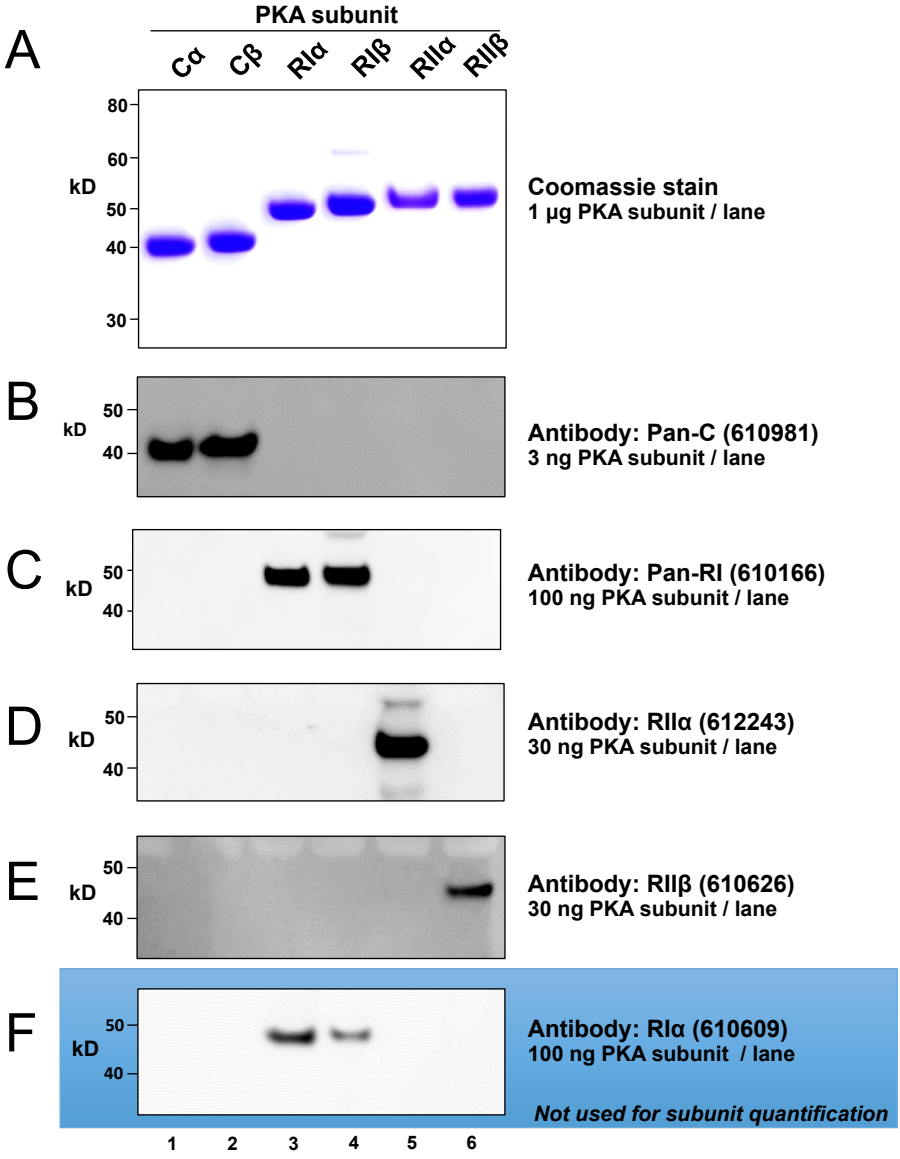
PKA subunit
A
Cα
Cβ
RIα
RIβ
RIIα
RIIβ
80
60
kD
50
40
30
Coomassie stain
1 µg PKA subunit / lane
B
kD
50
40
Antibody: Pan-C (610981)
3 ng PKA subunit / lane
C
kD
50
40
Antibody: Pan-RI (610166)
100 ng PKA subunit / lane
D
kD
50
40
Antibody: RIIα (612243)
30 ng PKA subunit / lane
E
kD
50
40
Antibody: RIIβ (610626)
30 ng PKA subunit / lane
F
kD
50
40
Antibody: RIα (610609)
100 ng PKA subunit / lane
Not used for subunit quantification
1
2
3
4
5
6

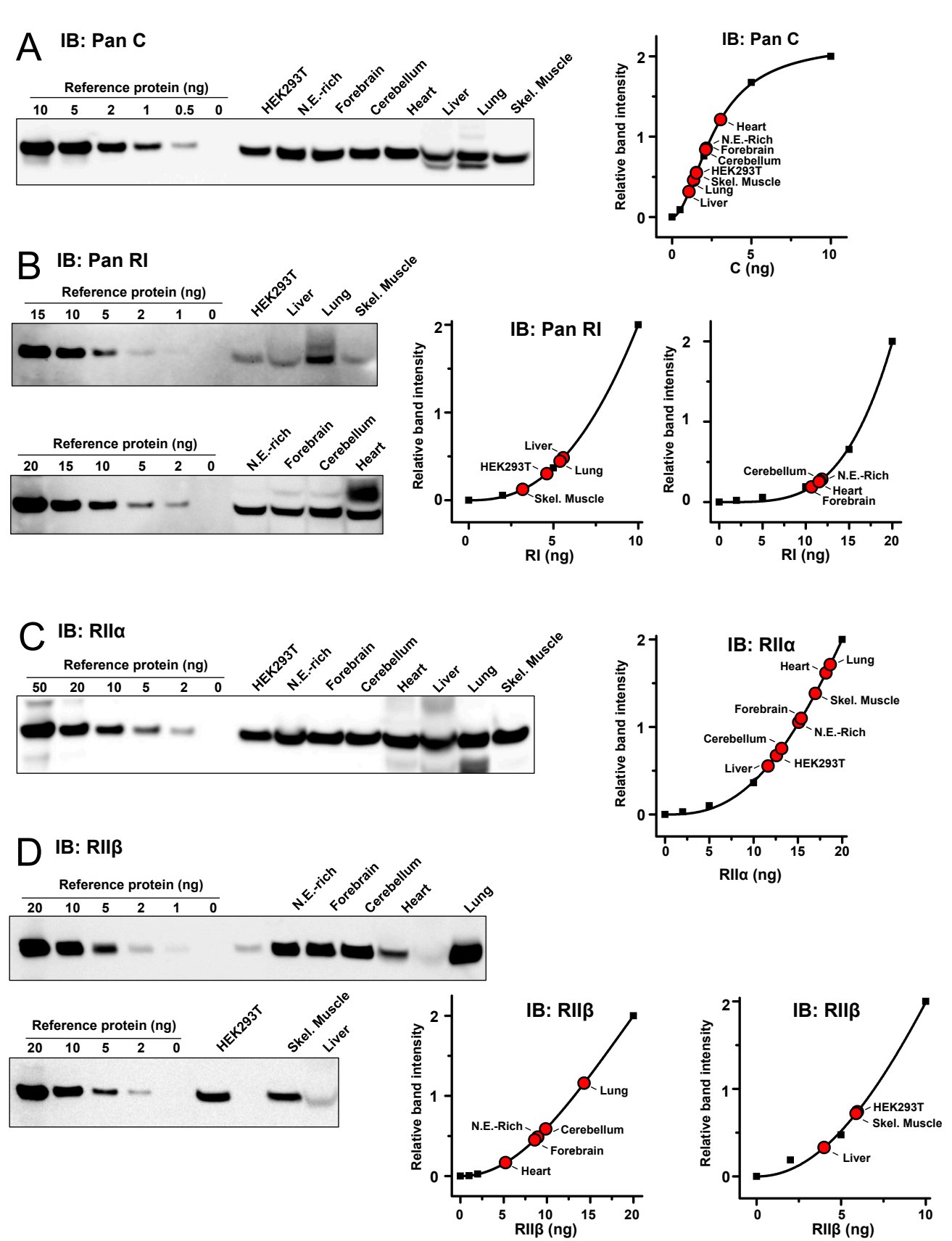
A
IB: Pan C
Reference protein (ng)
10 5 2 1 0.5 0
HEK293T
N.E.-rich
Forebrain
Cerebellum
Heart
Liver
Lung
Skel. Muscle
IB: Pan C
Relative band intensity
C (ng)
Heart
N.E.-Rich
Forebrain
Cerebellum
HEK293T
Skel. Muscle
Lung
Liver
B
IB: Pan RI
Reference protein (ng)
15 10 5 2 1 0
HEK293T
Liver
Lung
Skel. Muscle
Reference protein (ng)
20 15 10 5 2 0
N.E.-rich
Forebrain
Cerebellum
Heart
IB: Pan RI
Relative band intensity
RI (ng)
Liver
HEK293T
Lung
Skel. Muscle
Cerebellum
N.E.-Rich
Heart
Forebrain
C
IB: RIIα
Reference protein (ng)
50 20 10 5 2 0
HEK293T
N.E.-rich
Forebrain
Cerebellum
Heart
Liver
Lung
Skel. Muscle
IB: RIIα
Relative band intensity
RIIα (ng)
Heart
Lung
Skel. Muscle
Forebrain
N.E.-Rich
Cerebellum
HEK293T
Liver
D
IB: RIIβ
Reference protein (ng)
20 10 5 2 1 0
N.E.-rich
Forebrain
Cerebellum
Heart
Lung
Reference protein (ng)
20 10 5 2 0
HEK293T
Skel. Muscle
Liver
IB: RIIβ
Relative band intensity
RIIβ (ng)
Lung
N.E.-Rich
Cerebellum
Forebrain
Heart
IB: RIIβ
Relative band intensity
RIIβ (ng)
HEK293T
Skel. Muscle
Liver

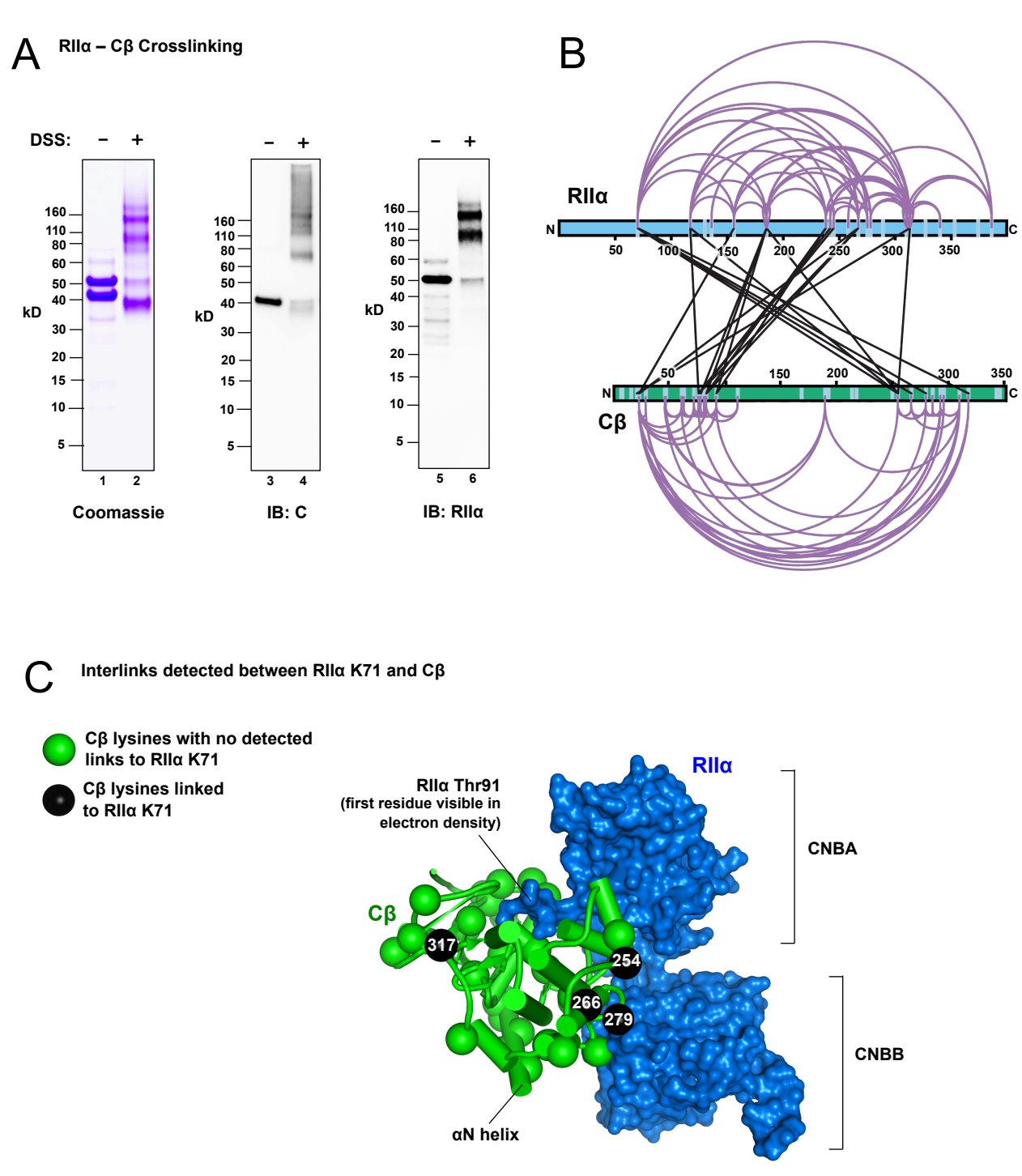
A
RIIα – Cβ Crosslinking
DSS:
– +
– +
– +
160
110
80
60
50
40
30
20
15
10
5
kD
1 2
3 4
5 6
Coomassie
IB: C
IB: RIIα
B
RIIα
N
C
50
100
150
200
250
300
350
Cβ
C
Interlinks detected between RIIα K71 and Cβ
Cβ lysines with no detected links to RIIα K71
Cβ lysines linked to RIIα K71
RIIα Thr91 (first residue visible in electron density)
RIIα
CNBA
CNBB
Cβ
317
254
266
279
αN helix

Table S1. Calculation of PKA subunit copy numbers per HEK293T cell. Copy numbers were determined according to the formula listed under the heading "Quantitative immunoblotting" in Supplemental Information. *The MW of Cα was used, since this is the predominant isoform in HEK293T cells according to the molecular weight detected with pan-C antibody (e.g., Fig 1*D*). **Average of RIα (42,982 Da) and RIβ (43,073 Da).

PKA Subunit	Fraction of HEK293T cell extract (ppm)	Subunit MW (Da)	Copies per g extract (x10^{18})	Copies per cell (x10^{6})
C	56.6±4	40590*	0.840±0.06	0.242±0.021
RI	183±34	43028**	2.56±0.48	0.734±0.13
RIIα	409±72	45518	5.41±0.95	1.54±0.23
RIIβ	82.9±21	46302	1.08±0.27	0.300±0.069

Table S2. XL-MS data following RIIβ-Cβ DSS crosslinking. The first column lists the amino acid sequence of crosslinked peptides and the positions of the crosslinked lysine residues. "deltaS" is a measure for how close the best assigned hit was scored in regard to the second best. The peptides are listed in order of "ID-Score", which is a weighted sum of different used to assess the quality of the composite MS2 spectrum as calculated by *xQuest*.

Crosslinked Peptide Sequence	Protein 1	Protein 2	Position 1	Position 2	deltaS	ID-score
FPSHFSSDLKDLLR-KGTAR-a10-b1	Cβ	RIIβ	266	46	0.36	49.45
RKGKSEVEENGAVEIAR-GQYFGELALVTNKPR-a2-b13	RIIβ	RIIβ	326	357	0	46.95
IIHPKTDDQR-LKVVDVIGTK-a5-b2	RIIβ	RIIβ	135	285	0.67	46.2
RKGKSEVEENGAVEIAR-GQYFGELALVTNKPR-a4-b13	RIIβ	RIIβ	328	357	0	45.47
LKQIEHTLNEK-ILDKQK-a2-b4	Cβ	Cβ	83	76	0.74	45.25
KGKSEVEENGAVEIAR-GQYFGELALVTNKPR-a3-b13	RIIβ	RIIβ	328	357	0	45.13
GKSEVEENGAVEIAR-GQYFGELALVTNKPR-a2-b13	RIIβ	RIIβ	328	357	0	45.12
ATEQYYAMKILDK-VMLVKHK-a9-b5	Cβ	Cβ	72	61	0.57	44.43
KMYESFIESLPFLK-IIVKNNAK-a1-b4	RIIβ	RIIβ	263	256	0	44
KGKSEVEENGAVEIAR-ITMKR-a1-b4	RIIβ	RIIβ	326	324	0.93	43.45
KGKSEVEENGAVEIAR-ITMKR-a3-b4	RIIβ	RIIβ	328	324	0.93	43.41
NLLQVDLTKR-IVSGKVR-a9-b5	Cβ	Cβ	279	254	0.47	43.36
IIHPKTDDQR-IIHPKTDDQR-a5-b5	RIIβ	RIIβ	135	135	0	43.03
NGVSDIKTHK-AKEDFLR-a7-b2	Cβ	Cβ	292	23	0.72	42.73
KMYESFIESLPFLK-KGTAR-a1-b1	RIIβ	RIIβ	263	46	0	42.2
LKVVDVIGTK-ITMKR-a2-b4	RIIβ	RIIβ	285	324	0	41.89
KMYESFIESLPFLK-NNAKKR-a1-b4	RIIβ	RIIβ	263	260	0	41.6
ATEQYYAMKILDK-VVKLK-a9-b3	Cβ	Cβ	72	81	0.48	40.88
KGKSEVEENGAVEIAR-KGTAR-a3-b1	RIIβ	RIIβ	328	44	0.45	40.87
RKMYESFIESLPFLK-IIVKNNAK-a2-b4	RIIβ	RIIβ	263	256	0.79	40.73
FPSHFSSDLKDLLR-AKEDFLR-a10-b2	Cβ	Cβ	266	23	0.58	40.68
IIHPKTDDQR-KGTAR-a5-b1	RIIβ	RIIβ	135	46	0	40.51
LVKDGEHVIDQGDDGDNFYVIDR-KGTAR-a3-b1	RIIβ	RIIβ	174	46	0	40.26
LKQIEHTLNEKR-ILDKQK-a11-b4	Cβ	Cβ	92	76	0	40.01
KGKSEVEENGAVEIAR-GQYFGELALVTNKPR-a1-b13	RIIβ	RIIβ	326	357	0	39.45
GKSEVEENGAVEIAR-ITMKRK-a2-b4	RIIβ	RIIβ	328	324	0.94	39.18
RKMYESFIESLPFLK-NNAKK-a2-b4	RIIβ	RIIβ	263	260	0.95	38.93
KGKSEVEENGAVEIAR-KGTAR-a1-b1	RIIβ	RIIβ	326	46	0.38	38.92
LKQIEHTLNEKR-AKEDFLR-a2-b2	Cβ	Cβ	83	23	0	38.7
LKVVDVIGTK-KGTAR-a2-b1	RIIβ	RIIβ	285	46	0	38.35
KGSEVESVKEFLAK-NGVSDIKTHK-a9-b7	Cβ	Cβ	16	292	0.93	38.18
KKTLGTGSFGR-VMLVKHK-a2-b5	Cβ	Cβ	47	61	0	38.12

LKVVDVIGTK-IIVKNNAK-a2-b4	RIIβ	RIIβ	285	256	0	37.95
IIHPKTDDQR-IIVKNNAK-a5-b4	RIIβ	RIIβ	135	256	0	37.55
KKTLGTGSFGR-VEAPFIPKFR-a2-b8	Cβ	Cβ	47	317	0.9	37.47
HKATEQYYAMKILDKQK-VVKLK-a11-b3	Cβ	Cβ	72	81	0.74	37.44
FGNLKNGVSDIKTHK-AKEDFLRK-a12-b2	Cβ	Cβ	292	23	0	37.21
FGNLKNGVSDIKTHK-AKEDFLR-a12-b2	Cβ	Cβ	292	23	0.27	37.12
KKTLGTGSFGR-KVEAPFIPKFR-a2-b9	Cβ	Cβ	47	317	0.77	36.83
KMYESFIESLPFLK-NNAKK-a1-b4	RIIβ	RIIβ	263	260	0	36.51
LKVVDVIGTK-RVKGR-a2-b3	RIIβ	Cβ	285	192	0	36.35
NGVSDIKTHK-AKEDFLRK-a7-b2	Cβ	Cβ	292	23	0.76	36.21
HKATEQYYAMKILDK-LKQIEHTLNEKR-a11-b2	Cβ	Cβ	72	83	0.26	36.19
GKSEVEENGAVEIAR-ITMKR-a2-b4	RIIβ	RIIβ	328	324	0.27	36.19
ILDKQK-VVKLK-a4-b3	Cβ	Cβ	76	81	0.89	36.05
LKQIEHTLNEKR-QKVVK-a2-b2	Cβ	Cβ	83	78	0	36.05
LKQIEHTLNEKR-ILDKQK-a2-b4	Cβ	Cβ	83	76	0.73	36.04
LKQIEHTLNEK-ILDKQKVVK-a2-b6	Cβ	Cβ	83	78	0.87	35.74
LKVVDVIGTK-NNAKK-a2-b4	RIIβ	RIIβ	285	260	0.79	35.65
KKTLGTGSFGR-KVEAPFIPKFR-a1-b9	Cβ	Cβ	46	317	0.71	35.1
LVKDGEHVIDQGDDGDNFYVIDR-IIVKNNAK-a3-b4	RIIβ	RIIβ	174	256	0.18	35
HKATEQYYAMKILDK-LKQIEHTLNEK-a11-b2	Cβ	Cβ	72	83	0.75	34.9
LVKDGEHVIDQGDDGDNFYVIDR-IVSGKVR-a3-b5	RIIβ	Cβ	174	254	0.32	34.82
GQYFGELALVTNKPR-ITMKR-a13-b4	RIIβ	RIIβ	357	324	0	34.79
NGVSDIKTHKWFATTDWIAIYQR-AKEDFLR-a10-b2	Cβ	Cβ	295	23	0.26	34.64
RKMYESFIESLPFLK-ILDKQK-a2-b4	RIIβ	Cβ	263	76	0.69	34.62
GQYFGELALVTNKPR-KGTAR-a13-b1	RIIβ	RIIβ	357	46	0	34.42
QIEHTLNEKR-ILDKQK-a9-b4	Cβ	Cβ	92	76	0	34.25
LKQIEHTLNEKR-ILDKQKVVK-a2-b6	Cβ	Cβ	83	78	0	34.16
KMYESFIESLPFLK-RVKGR-a1-b3	RIIβ	Cβ	263	192	0.37	33.91
LVKDGEHVIDQGDDGDNFYVIDR-RIIVKNNAK-a3-b5	RIIβ	RIIβ	174	256	0	33.79
NGVSDIKTHK-KVEAPFIPK-a7-b1	Cβ	Cβ	292	309	0.81	33.79
KGSEVESVKEFLAK-AKEDFLR-a9-b2	Cβ	Cβ	16	23	0.77	33.42
LKQIEHTLNEK-QKVVK-a2-b2	Cβ	Cβ	83	78	0.77	33.38
QIEHTLNEKR-AKEDFLR-a9-b2	Cβ	Cβ	92	23	0	33.34
LKVVDVIGTK-VVKLK-a2-b3	RIIβ	Cβ	285	81	0.38	33.24
RKGKSEVEENGAVEIAR-ITMKR-a4-b4	RIIβ	RIIβ	328	324	0.33	33.1
RKGKSEVEENGAVEIAR-ITMKR-a2-b4	RIIβ	RIIβ	326	324	0.31	32.73
HKATEQYYAMKILDK-VVKLK-a11-b3	Cβ	Cβ	72	81	0.57	32.69
HKATEQYYAMK-KKTLGTGSFGR-a2-b2	Cβ	Cβ	63	47	0.52	32.69
HKATEQYYAMKILDKQK-AKEDFLR-a11-b2	Cβ	Cβ	72	23	0.74	32.64
LVKDGEHVIDQGDDGDNFYVIDR-IIHPKTDDQR-a3-b5	RIIβ	RIIβ	174	135	0.69	32.57
KWENPPPSNAGLEDFER-KVEAPFIPK-a1-b1	Cβ	Cβ	29	309	0	31.72
ATEQYYAMKILDK-LKQIEHTLNEKR-a9-b2	Cβ	Cβ	72	83	0.37	31.56
MYESFIESLPFLKSLEFSER-KGTAR-a13-b1	RIIβ	RIIβ	276	46	0	31.48

KGKSEVEENGAVEIAR-NNAKK-a3-b4	RIIβ	RIIβ	328	260	0.56	31.08
ATEQYYAMKILDK-LKQIEHTLNEKR-a9-b11	Cβ	Cβ	72	92	0.21	31.06
FPSHFSSDLKDLLR-IVSGKVR-a10-b5	Cβ	Cβ	266	254	0.73	30.91
KMYESFIESLPFLK-NNAKKR-a1-b5	RIIβ	RIIβ	263	261	0.92	30.9
KWENPPPSNAGLEDFER-NGVSDIKTHK-a1-b7	Cβ	Cβ	29	292	0	30.77
AKEDFLR-RVKGR-a2-b3	Cβ	Cβ	23	192	0	30.56
KVEAPFIPK-AKEDFLR-a1-b2	Cβ	Cβ	309	23	0	30.51
ATEQYYAMKILDK-LKQIEHTLNEK-a9-b2	Cβ	Cβ	72	83	0.36	29.82
ATEQYYAMKILDK-QIEHTLNEKR-a9-b9	Cβ	Cβ	72	92	0	29.68
AKEDFLRK-RVKGR-a2-b3	Cβ	Cβ	23	192	0.51	29.63
ATEQYYAMKILDK-RVKGR-a9-b3	Cβ	Cβ	72	192	0.6	29.39
KWENPPPSNAGLEDFER-AKEDFLR-a1-b2	Cβ	Cβ	29	23	0.9	29.07
FGNLKNGVSDIKTHK-KGSEVESVKEFLAK-a12-b9	Cβ	Cβ	292	16	0.82	28.68
KMYESFIESLPFLK-LKVVDVIGTK-a1-b2	RIIβ	RIIβ	263	285	0	28.64
DLKPENLLIDHQGYIQVTDFGFAKR-AKEDFLR-a24-b2	Cβ	Cβ	189	23	0.37	28.33
GQYFGELALVTNKPRAASAHAIGTVK-LKQIEHTLNEKR-a13-b11	RIIβ	Cβ	357	92	0.21	28.11
KMYESFIESLPFLKSLEFSER-KGTAR-a14-b1	RIIβ	RIIβ	276	46	0.3	27.76
LKQIEHTLNEKR-RVKGR-a2-b3	Cβ	Cβ	83	192	0	27.69
KWENPPPSNAGLEDFER-IVSGKVR-a1-b5	Cβ	Cβ	29	254	0	27.65
QIEHTLNEKR-VVKLK-a9-b3	Cβ	Cβ	92	81	0.32	27.61
LKQIEHTLNEKR-ILDKQKVVK-a2-b4	Cβ	Cβ	83	76	0.88	27.54
RFGNLKNGVSDIKTHK-AKEDFLR-a13-b2	Cβ	Cβ	292	23	0.58	27.51
LEYSFKDNSNLYMVMEYVPGGEMFSHLR-ILDKQK-a6-b4	Cβ	Cβ	111	76	0	27.34
KWENPPPSNAGLEDFER-ATEQYYAMKILDKQK-a1-b13	Cβ	Cβ	29	76	0.35	26.82
KWENPPPSNAGLEDFER-LKQIEHTLNEKR-a1-b11	Cβ	Cβ	29	92	0	26.52
HKATEQYYAMKILDK-LKQIEHTLNEKR-a11-b11	Cβ	Cβ	72	92	0.36	26.39
KMYESFIESLPFLK-RIIVKNNAK-a1-b5	RIIβ	RIIβ	263	256	0.87	25.21
ATEQYYAMKILDKQK-LKQIEHTLNEKR-a9-b2	Cβ	Cβ	72	83	0.69	25.18
KWENPPPSNAGLEDFER-LKQIEHTLNEKR-a1-b2	Cβ	Cβ	29	83	0	25.17
FGNLKNGVSDIKTHK-NLLQVDLTKR-a5-b9	Cβ	Cβ	285	279	0.38	25.16
FPSHFSSDLKDLLRNLLQVDLTKR-IVSGKVR-a10-b5	Cβ	Cβ	266	254	0.56	25.13
GQYFGELALVTNKPR-FGNLKNGVSDIK-a13-b5	RIIβ	Cβ	357	285	0.33	24.94
NLLQVDLTKRFGNLK-NGVSDIKTHK-a9-b7	Cβ	Cβ	279	292	0.91	24.68
GQYFGELALVTNKPRAASAHAIGTVK-LKQIEHTLNEKR-a13-b2	RIIβ	Cβ	357	83	0.17	24.65
LKQIEHTLNEK-RVKGR-a2-b3	Cβ	Cβ	83	192	0.49	24.35
ATEQYYAMKILDK-QKVVKLK-a9-b5	Cβ	Cβ	72	81	0.9	23.59
KWENPPPSNAGLEDFER-QIEHTLNEKR-a1-b9	Cβ	Cβ	29	92	0.35	23.45
ATEQYYAMKILDKQK-NGVSDIKTHK-a13-b7	Cβ	Cβ	76	292	0.93	22.86
HKATEQYYAMKILDK-QIEHTLNEKR-a11-b9	Cβ	Cβ	72	92	0.4	22.67

LKQIEHTLNEK-LKVVDVIGTK-a2-b2	Cβ	RIIβ	83	285	0.5	22.52
RKMYESFIESLPFLKSLEFSER-KGTAR-a15-b1	RIIβ	RIIβ	276	46	0	22.27
HKATEQYYAMKILDKQK-QIEHTLNEKR-a11-b9	Cβ	Cβ	72	92	0.76	22.07
HKATEQYYAMKILDKQK-LKQIEHTLNEKR-a11-b2	Cβ	Cβ	72	83	0.71	21.62
RKMYESFIESLPFLKSLEFSER-IIVKNNAK-a15-b4	RIIβ	RIIβ	276	256	0.82	21.54
NLDPEQMSQVLDAMFEKLVK-IIHPKTDDQR-a17-b5	RIIβ	RIIβ	171	135	0.53	21.33
LKQIEHTLNEKR-AKEDFLR-a11-b2	Cβ	Cβ	92	23	0	21.26
ATEQYYAMKILDKQK-VVKLK-a9-b3	Cβ	Cβ	72	81	0.81	20.99
LKQIEHTLNEKR-HKATEQYYAMK-a2-b2	Cβ	Cβ	83	63	0	20.88
NGVSDIKTHK-QIEHTLNEKR-a7-b9	Cβ	Cβ	292	92	0	20.68
QIEHTLNEKR-ILDKQKVVK-a9-b4	Cβ	Cβ	92	76	0.91	20.34
KWENPPPSNAGLEDFER-KKTLGTGSFGR-a1-b2	Cβ	Cβ	29	47	0.36	20.14

Table S3. XL-MS data following RIIβ-Cβ-AKAP18α DSS crosslinking. The first column lists the amino acid sequence of crosslinked peptides and the positions of the crosslinked lysine residues. "deltaS" is a measure for how close the best assigned hit was scored in regard to the second best. The peptides are listed in order of "ID-Score", which is a weighted sum of different used to assess the quality of the composite MS2 spectrum as calculated by *xQuest*.

Crosslinked Peptide Sequence	Protein 1	Protein 2	Position 1	Position 2	deltaS	ID-score
LKQIEHTLNEK-ILDKQK-a2-b4	Cβ	Cβ	83	76	0.52	50.16
GKSEVEENGAVEIAR-GQYFGELALVTNKPR-a2-b13	RIIβ	RIIβ	328	357	0	45.44
RKGKSEVEENGAVEIAR-GQYFGELALVTNKPR-a2-b13	RIIβ	RIIβ	326	357	0	44.79
KMYESFIESLPFLK-NNAKKR-a1-b4	RIIβ	RIIβ	263	260	0.4	44.5
IIHPKTDDQR-LKVVDVIGTK-a5-b2	RIIβ	RIIβ	135	285	0	44.42
FPSHFSSDLKDLLR-KGTAR-a10-b1	Cβ	RIIβ	266	46	0.48	44.41
NLLQVDLTKR-IVSGKVR-a9-b5	Cβ	Cβ	279	254	0.63	42.61
KMYESFIESLPFLK-IIVKNNAK-a1-b4	RIIβ	RIIβ	263	256	0	42.35
HKATEQYYAMKILDKQK-VVKLK-a11-b3	Cβ	Cβ	72	81	0.76	42.24
NGVSDIKTHK-AKEDFLR-a7-b2	Cβ	Cβ	292	23	0	41.27
KGKSEVEENGAVEIAR-ITMKR-a1-b4	RIIβ	RIIβ	326	324	0.94	41.25
ILDKQK-VVKLK-a4-b3	Cβ	Cβ	76	81	0.88	41.17
KGKSEVEENGAVEIAR-ITMKR-a3-b4	RIIβ	RIIβ	328	324	0.94	41.05
KGSEVESVKEFLAK-NGVSDIKTHK-a9-b7	Cβ	Cβ	16	292	0.57	40.47
KKTLGTGSFGR-VEAPFIPKFR-a2-b8	Cβ	Cβ	47	317	0.92	40.23
LKQIEHTLNEKR-ILDKQK-a11-b4	Cβ	Cβ	92	76	0	40.07
LKQIEHTLNEK-AKEDFLR-a2-b2	Cβ	Cβ	83	23	0.6	38.43
KKTLGTGSFGR-VMLVKHK-a2-b5	Cβ	Cβ	47	61	0	38.36
AKEDFLRK-RVKGR-a2-b3	Cβ	Cβ	23	192	0.52	37.98
LKVVDVIGTK-KGTAR-a2-b1	RIIβ	RIIβ	285	46	0	37.96
LVKDGEHVIDQGDDGDNFYVIDR-KGTAR-a3-b1	RIIβ	RIIβ	174	46	0	37.89
ATEQYYAMKILDK-VMLVKHK-a9-b5	Cβ	Cβ	72	61	0.56	37.59
LKQIEHTLNEKR-AKEDFLR-a11-b2	Cβ	Cβ	92	23	0	37.04
LVKDGEHVIDQGDDGDNFYVIDR-IIVKNNAK-a3-b4	RIIβ	RIIβ	174	256	0.22	36.73
KMYESFIESLPFLK-KGTAR-a1-b1	RIIβ	RIIβ	263	46	0	36.55
LKQIEHTLNEKR-ILDKQKVVK-a2-b6	Cβ	Cβ	83	78	0.88	36.5
KVEAPFIPKFR-AKEDFLR-a9-b2	Cβ	Cβ	317	23	0.36	36.29
IIHPKTDDQR-KGTAR-a5-b1	RIIβ	RIIβ	135	46	0.46	35.89
LKVVDVIGTK-NNAKK-a2-b4	RIIβ	RIIβ	285	260	0	35.82
HKATEQYYAMKILDK-LKQIEHTLNEKR-a11-b2	Cβ	Cβ	72	83	0.43	35.37
LVKDGEHVIDQGDDGDNFYVIDR-IVSGKVR-a3-b5	RIIβ	Cβ	174	254	0.17	34.9
LKVVDVIGTK-IIVKNNAK-a2-b4	RIIβ	RIIβ	285	256	0	34.62
HKATEQYYAMKILDK-LKQIEHTLNEKR-a11-	Cβ	Cβ	72	92	0.32	34.59

b11

HKATEQYYAMKILDKQK-AKEDFLR-a11-b2	Cβ	Cβ	72	23	0.68	34.29
HKATEQYYAMK-AKEDFLR-a2-b2	Cβ	Cβ	63	23	0	33.97
KGSEVESVKEFLAK-AKEDFLR-a9-b2	Cβ	Cβ	16	23	0.7	33.9
LVKDGEHVIDQGDDGDNFYVIDR-IIHPKTDDQR-a3-b5	RIIβ	RIIβ	174	135	0	33.36
AKEDFLR-VMLVKHK-a2-b5	Cβ	Cβ	23	61	0	33.36
IIHPKTDDQR-IIVKNNAK-a5-b4	RIIβ	RIIβ	135	256	0	33.19
HKATEQYYAMK-ILDKQK-a2-b4	Cβ	Cβ	63	76	0	32.97
VMLVKHK-ILDKQK-a5-b4	Cβ	Cβ	61	76	0	32.54
GQYFGELALVTNKPR-KGTAR-a13-b1	RIIβ	RIIβ	357	46	0	32.41
KKTLGTGSFGR-KVEAPFIPKFR-a1-b9	Cβ	Cβ	46	317	0.79	32.41
NGVSDIKTHK-KVEAPFIPK-a7-b1	Cβ	Cβ	292	309	0	32.36
KWENPPPSNAGLEDFER-NGVSDIKTHK-a1-b7	Cβ	Cβ	29	292	0.31	32.19
KWENPPPSNAGLEDFER-ILDKQK-a1-b4	Cβ	Cβ	29	76	0	32.07
DLKPENLLIDHQGYIQVTDFGFAKR-AKEDFLR-a24-b2	Cβ	Cβ	189	23	0.29	32.03
FGNLKNGVSDIK-AKEDFLR-a5-b2	Cβ	Cβ	285	23	0	31.84
LKQIEHTLNEKR-ILDKQKVVK-a11-b6	Cβ	Cβ	92	78	0.75	31.51
LKVVDVIGTK-VVKLK-a2-b3	RIIβ	Cβ	285	81	0	31.35
KWENPPPSNAGLEDFER-KVEAPFIPK-a1-b1	Cβ	Cβ	29	309	0.42	30.72
LKQIEHTLNEKR-HKATEQYYAMK-a2-b2	Cβ	Cβ	83	63	0.4	30.52
QIEHTLNEKR-VVKLK-a9-b3	Cβ	Cβ	92	81	0	29.73
KVEAPFIPK-AKEDFLR-a1-b2	Cβ	Cβ	309	23	0	29.51
LKQIEHTLNEKR-HKATEQYYAMK-a11-b2	Cβ	Cβ	92	63	0	29.29
LKVVDVIGTK-ITMKR-a2-b4	RIIβ	RIIβ	285	324	0	28.93
NLLQVDLTKRFGNLK-NGVSDIKTHK-a9-b7	Cβ	Cβ	279	292	0.91	27.85
KMYESFIESLPFLKSLEFSER-KGTAR-a14-b1	RIIβ	RIIβ	276	46	0.36	27.07
NGVSDIKTHK-EFLAKAK-a7-b5	Cβ	Cβ	292	21	0.72	26.75
KWENPPPSNAGLEDFER-LKQIEHTLNEKR-a1-b11	Cβ	Cβ	29	92	0.28	26.43
NGVSDIKTHK-QIEHTLNEKR-a7-b9	Cβ	Cβ	292	92	0.7	26.17
HKATEQYYAMKILDKQK-KWENPPPSNAGLEDFER-a11-b1	Cβ	Cβ	72	29	0.51	25.99
KMYESFIESLPFLK-LKVVDVIGTK-a1-b2	RIIβ	RIIβ	263	285	0.48	25.77
FGNLKNGVSDIK-ICEKDR-a5-b4	Cβ	AKAP18α	285	19	0.86	24.44
ATEQYYAMKILDKQK-NGVSDIKTHK-a13-b7	Cβ	Cβ	76	292	0.94	24.39
QIEHTLNEKR-VMLVKHK-a9-b5	Cβ	Cβ	92	61	0	24
KWENPPPSNAGLEDFER-LKQIEHTLNEKR-a1-b2	Cβ	Cβ	29	83	0	23.73
FGNLKNGVSDIKTHK-KGSEVESVKEFLAK-a5-b9	Cβ	Cβ	285	16	0.54	23.66
KGSEVESVKEFLAKAK-ILDKQK-a9-b4	Cβ	Cβ	16	76	0.89	22.35
KWENPPPSNAGLEDFER-HKATEQYYAMK-a1-b2	Cβ	Cβ	29	63	0.24	22.01
ATEQYYAMKILDKQK-NGVSDIKTHK-a9-b7	Cβ	Cβ	72	292	0.38	21.23
AVQQYLEETQNKKQPGEGNSTKAEEGDR-KMYESFIESLPFLK-a22-b1	AKAP18α	RIIβ	65	263	0	21.07
ATEQYYAMKILDK-EFLAKAK-a9-b5	Cβ	Cβ	72	21	0	20.79
FGNLKNGVSDIKTHK-NLLQVDLTKR-a5-b9	Cβ	Cβ	285	279	0.65	20.68
KTLGTGSFGRVMLVK-ILDKQK-a1-b4	Cβ	Cβ	47	76	0.77	20.65

Table S4. XL-MS data following RIIα-Cβ DSS crosslinking. The first column lists the amino acid sequence of crosslinked peptides and the positions of the crosslinked lysine residues. "deltaS" is a measure for how close the best assigned hit was scored in regard to the second best. The peptides are listed in order of "ID-Score", which is a weighted sum of different used to assess the quality of the composite MS2 spectrum as calculated by *xQuest*.

Crosslinked Peptide Sequence	Protein 1	Protein 2	Position 1	Position 2	deltaS	ID-score
TKSNKDGGNQEVEIAR-SNKDGGNQEVEIAR-a2-b3	RIIα	RIIα	311	314	0.75	54.11
KMFESFIESVPLLK-MKIVDVIGEK-a1-b2	RIIα	RIIα	246	268	0	49.14
NISHYEEQLVKMFGSSVDLGNLGQ-TKSNKDGGNQEVEIAR-a11-b5	RIIα	RIIα	387	314	0	48.79
NISHYEEQLVKMFGSSVDLGNLGQ-TKSNKDGGNQEVEIAR-a11-b2	RIIα	RIIα	387	311	0	47.93
KVEAPFIPK-AKEDFLR-a1-b2	Cβ	Cβ	309	23	0	47.4
SNKDGGNQEVEIAR-SNKDGGNQEVEIAR-a3-b3	RIIα	RIIα	314	314	0	45.9
NLLQVDLTKR-IVSGKVR-a9-b5	Cβ	Cβ	279	254	0.42	45.65
TKSNKDGGNQEVEIAR-SNKDGGNQEVEIAR-a5-b3	RIIα	RIIα	314	314	0.88	44.6
NISHYEEQLVKMFGSSVDLGNLGQ-SNKDGGNQEVEIAR-a11-b3	RIIα	RIIα	387	314	0	43.7
MKIVDVIGEK-ILDKQK-a2-b4	RIIα	Cβ	268	76	0	43.25
MKIVDVIGEK-IYKDGER-a2-b3	RIIα	RIIα	268	279	0	42.83
TKSNKDGGNQEVEIAR-TKSNKDGGNQEVEIAR-a2-b2	RIIα	RIIα	311	311	0.79	42.79
TKSNKDGGNQEVEIAR-VIHPKTDEQR-a5-b5	RIIα	RIIα	314	118	0.4	41.46
TKSNKDGGNQEVEIAR-TKSNKDGGNQEVEIAR-a5-b5	RIIα	RIIα	314	314	0.8	41.38
SNKDGGNQEVEIAR-IYKDGER-a3-b3	RIIα	RIIα	314	279	0	41.36
LKQIEHTLNEKR-ILDKQK-a11-b4	Cβ	Cβ	92	76	0	41.14
KMFESFIESVPLLK-IIVKNNAK-a1-b4	RIIα	RIIα	246	239	0	41.05
FGNLKNGVSDIKTHK-AKEDFLR-a12-b2	Cβ	Cβ	292	23	0	40.92
VIHPKTDEQR-RIIVKNNAK-a5-b5	RIIα	RIIα	118	239	0	40.91
HKATEQYYAMK-KKTLGTGSFGR-a2-b2	Cβ	Cβ	63	47	0	40.69
LKQIEHTLNEK-ILDKQKVVK-a2-b6	Cβ	Cβ	83	78	0.94	40.49
LKQIEHTLNEK-ILDKQK-a2-b4	Cβ	Cβ	83	76	0	40.14
LKQIEHTLNEKR-MKIVDVIGEK-a2-b2	Cβ	RIIα	83	268	0	40.12
GTYDILVTKDNQTR-MKIVDVIGEKIYK-a9-b2	RIIα	RIIα	186	268	0.59	39.88
GTYDILVTKDNQTR-MKIVDVIGEK-a9-b2	RIIα	RIIα	186	268	0.57	39.83
RNISHYEEQLVKMFGSSVDLGNLGQ-TKSNKDGGNQEVEIAR-a12-b5	RIIα	RIIα	387	314	0.5	39.16
RKMFESFIESVPLLK-IIVKNNAK-a2-b4	RIIα	RIIα	246	239	0.82	39.06
VIHPKTDEQR-IIVKNNAK-a5-b4	RIIα	RIIα	118	239	0	38.1
KKTLGTGSFGR-VEAPFIPKFR-a2-b8	Cβ	Cβ	47	317	0.79	37.97
TKSNKDGGNQEVEIAR-VIHPKTDEQR-a2-b5	RIIα	RIIα	311	118	0.4	37.5
KVEAPFIPKFR-VMLVKHK-a9-b5	Cβ	Cβ	317	61	0	37.29
AKEDFLR-VMLVKHK-a2-b5	Cβ	Cβ	23	61	0	37.08
KKTLGTGSFGR-VMLVKHK-a2-b5	Cβ	Cβ	47	61	0	36.98
DLKPENLLIDHQGYIQVTDFGFAKR-AKEDFLR-a24-b2	Cβ	Cβ	189	23	0.36	36.83
LKQIEHTLNEKR-ILDKQKVVK-a2-b6	Cβ	Cβ	83	78	0.67	36.64

KMFESFIESVPLLK-NNAKKR-a1-b4	RIIα	RIIα	246	243	0	36.54
TKSNKDGGNQEVEIAR-IYKDGER-a2-b3	RIIα	RIIα	311	279	0.22	36.37
LKQIEHTLNEKR-ILDKQK-a2-b4	Cβ	Cβ	83	76	0	36.2
NGVSDIKTHK-AKEDFLR-a7-b2	Cβ	Cβ	292	23	0	36.01
THKWFATTDWIAIYQR-FGNLKNGVSDIK-a3-b5	Cβ	Cβ	295	285	0	35.7
NGVSDIKTHK-AKEDFLRK-a7-b2	Cβ	Cβ	292	23	0.64	35.66
LKQIEHTLNEKR-ILDKQKVVK-a2-b4	Cβ	Cβ	83	76	0.73	35.37
VIHPKTDEQR-IYKDGER-a5-b3	RIIα	RIIα	118	279	0	35.32
GTYDILVTKDNQTR-GTYDILVTKDNQTR-a9-b9	RIIα	RIIα	186	186	0.82	35.11
RKMFESFIESVPLLK-IIVKNNAKK-a2-b8	RIIα	RIIα	246	243	0.47	35
TKSNKDGGNQEVEIAR-GTYDILVTKDNQTR-a5-b9	RIIα	RIIα	314	186	0.69	34.86
IVKADEHVIDQGDDGDNFYVIER-MKIVDVIGEK-a3-b2	RIIα	RIIα	157	268	0	34.71
SNKDGGNQEVEIAR-IIVKNNAK-a3-b4	RIIα	RIIα	314	239	0	34.7
VIHPKTDEQR-ILDKQK-a5-b4	RIIα	Cβ	118	76	0	34.68
TKSNKDGGNQEVEIAR-MKIVDVIGEK-a2-b2	RIIα	RIIα	311	268	0.44	34.62
GTYDILVTKDNQTR-VIHPKTDEQR-a9-b5	RIIα	RIIα	186	118	0.5	34.53
IVKADEHVIDQGDDGDNFYVIER-VIHPKTDEQR-a3-b5	RIIα	RIIα	157	118	0.41	34.48
FPSHFSSDLKDLLR-IVSGKVR-a10-b5	Cβ	Cβ	266	254	0	34.44
GTYDILVTKDNQTR-SNKDGGNQEVEIAR-a9-b3	RIIα	RIIα	186	314	0.62	34.29
SNKDGGNQEVEIAR-NNAKKR-a3-b4	RIIα	RIIα	314	243	0	34.29
KKTLGTGSFGR-KVEAPFIPKFR-a2-b9	Cβ	Cβ	47	317	0	34.05
KKTLGTGSFGR-VMLVKHK-a1-b5	Cβ	Cβ	46	61	0	33.96
NGVSDIKTHKWFATTDWIAIYQR-AKEDFLR-a10-b2	Cβ	Cβ	295	23	0	33.93
GTYDILVTKDNQTR-IVSGKVR-a9-b5	RIIα	Cβ	186	254	0.54	33.77
TKSNKDGGNQEVEIAR-MKIVDVIGEK-a5-b2	RIIα	RIIα	314	268	0.44	33.75
FGNLKNGVSDIK-NLLQVDLTKR-a5-b9	Cβ	Cβ	285	279	0	33.45
TKSNKDGGNQEVEIAR-IYKDGER-a5-b3	RIIα	RIIα	314	279	0.34	33.43
NGVSDIKTHKWFATTDWIAIYQR-AKEDFLR-a7-b2	Cβ	Cβ	292	23	0	33.38
MKIVDVIGEK-AKEDFLR-a2-b2	RIIα	Cβ	268	23	0	33.33
DILLFKNLDQEQLSQVLDAMFER-IYKDGER-a6-b3	RIIα	RIIα	137	279	0	33.32
IVDVIGEKIYKDGER-GTYDILVTKDNQTR-a8-b9	RIIα	RIIα	276	186	0.64	33.26
LKQIEHTLNEKR-AKEDFLR-a2-b2	Cβ	Cβ	83	23	0	33.21
SNKDGGNQEVEIAR-VIHPKTDEQR-a3-b5	RIIα	RIIα	314	118	0	33.18
HKATEQYYAMKILDK-LKQIEHTLNEKR-a11-b2	Cβ	Cβ	72	83	0.66	33.12
TKSNKDGGNQEVEIAR-GQYFGELALVTNKPR-a5-b13	RIIα	RIIα	314	341	0.79	33.05
TKSNKDGGNQEVEIAR-IIVKNNAK-a2-b4	RIIα	RIIα	311	239	0	32.91
FGNLKNGVSDIKTHK-AKEDFLRK-a12-b2	Cβ	Cβ	292	23	0.37	32.78
VADAKGDSESEEDEDLEVPVPSR-NLLQVDLTKR-a5-b9	RIIα	Cβ	71	279	0	32.74
RNISHYEEQLVKMFGSSVDLGNLGQ-TKSNKDGGNQEVEIAR-a12-b2	RIIα	RIIα	387	311	0.65	32.55
KVEAPFIPK-ILDKQK-a1-b4	Cβ	Cβ	309	76	0	32.38
KWENPPPSNAGLEDFER-AKEDFLR-a1-b2	Cβ	Cβ	29	23	0.24	32.34
KTLGTGSFGR-VMLVKHK-a1-b5	Cβ	Cβ	47	61	0	32.16
FPSHFSSDLKDLLR-NLLQVDLTKR-a10-b9	Cβ	Cβ	266	279	0.81	32.16
VVKLKQIEHTLNEK-ILDKQK-a3-b4	Cβ	Cβ	81	76	0.95	32.11
HKATEQYYAMK-KKTLGTGSFGR-a2-b1	Cβ	Cβ	63	46	0.55	32.07
ATEQYYAMKILDK-VMLVKHK-a9-b5	Cβ	Cβ	72	61	0	31.86
IVKADEHVIDQGDDGDNFYVIER-GTYDILVTKDNQTR-a3-b9	RIIα	RIIα	157	186	0.54	31.84
QIEHTLNEKR-ILDKQK-a9-b4	Cβ	Cβ	92	76	0.79	31.8
RKMFESFIESVPLLK-IIVKNNAKK-a2-b4	RIIα	RIIα	246	239	0	31.66

TKSNKDGGNQEVEIAR-GQYFGELALVTNKPR-a2-b13	RIIα	RIIα	311	341	0	31.65
GQYFGELALVTNKPR-SNKDGGNQEVEIAR-a13-b3	RIIα	RIIα	341	314	0	31.54
NGVSDIKTHK-KVEAPFIPK-a7-b1	Cβ	Cβ	292	309	0	31.26
FGNLKNGVSDIKTHK-NLLQVDLTKR-a5-b9	Cβ	Cβ	285	279	0.79	31.19
QSLGHPPPEPGPDRVADAKGDSESEEDEDLEVPVPSR-GTYDILVTKDNQTR-a19-b9	RIIα	RIIα	71	186	0.67	31.01
TKSNKDGGNQEVEIAR-GTYDILVTKDNQTR-a2-b9	RIIα	RIIα	311	186	0.77	30.84
QIEHTLNEKR-AKEDFLR-a9-b2	Cβ	Cβ	92	23	0	30.7
LKQIEHTLNEKR-ILDKQKVVK-a11-b6	Cβ	Cβ	92	78	0.81	30.53
KVEAPFIPKFR-AKEDFLR-a9-b2	Cβ	Cβ	317	23	0.58	30.17
KTLGTGSFGR-VEAPFIPKFR-a1-b8	Cβ	Cβ	47	317	0	30.16
LKQIEHTLNEKR-IIVKNNAK-a2-b4	Cβ	RIIα	83	239	0.58	30.08
GTYDILVTKDNQTR-ILDKQKVVK-a9-b6	RIIα	Cβ	186	78	0.93	29.97
TKSNKDGGNQEVEIAR-NNAKKR-a2-b4	RIIα	RIIα	311	243	0.52	29.59
VADAKGDSESEEDEDLEVPVPSR-IVSGKVR-a5-b5	RIIα	Cβ	71	254	0	29.55
SNKDGGNQEVEIAR-MKIVDVIGEK-a3-b2	RIIα	RIIα	314	268	0	29.5
VIHPKTDEQR-ILDKQKVVK-a5-b4	RIIα	Cβ	118	76	0	29.25
IVDVIGEKIYKDGER-IIVKNNAK-a8-b4	RIIα	RIIα	276	239	0	29.15
MKIVDVIGEK-IIVKNNAK-a2-b4	RIIα	RIIα	268	239	0	28.97
LKQIEHTLNEKR-ILDKQKVVK-a11-b4	Cβ	Cβ	92	76	0	28.66
LEYSFKDNSNLYMVMEYVPGGEMFSHLR-QIEHTLNEKR-a6-b9	Cβ	Cβ	111	92	0.22	28.59
ATEQYYAMKILDK-AKEDFLR-a9-b2	Cβ	Cβ	72	23	0	28.58
GTYDILVTKDNQTR-IIVKNNAK-a9-b4	RIIα	RIIα	186	239	0.49	28
VADAKGDSESEEDEDLEVPVPSR-KMFESFIESVPLLK-a5-b1	RIIα	RIIα	71	246	0	27.74
SNKDGGNQEVEIAR-EFLAKAK-a3-b5	RIIα	Cβ	314	21	0	27.72
SNKDGGNQEVEIAR-IVSGKVR-a3-b5	RIIα	Cβ	314	254	0	27.63
VIHPKTDEQR-IVSGKVR-a5-b5	RIIα	Cβ	118	254	0	27.54
QSLGHPPPEPGPDRVADAKGDSESEEDEDLEVPVPSR-NLLQVDLTKR-a19-b9	RIIα	Cβ	71	279	0	27.5
VADAKGDSESEEDEDLEVPVPSRFNR-GTYDILVTKDNQTR-a5-b9	RIIα	RIIα	71	186	0.46	27.31
IVKADEHVIDQGDDGDNFYVIER-VADAKGDSESEEDEDLEVPVPSR-a3-b5	RIIα	RIIα	157	71	0.71	27.25
NISHYEEQLVKMFGSSVDLGNLGQ-KMFESFIESVPLLKSLEVSER-a11-b14	RIIα	RIIα	387	259	0.46	27.15
QIEHTLNEKR-IIVKNNAK-a9-b4	Cβ	RIIα	92	239	0	26.99
QSLGHPPPEPGPDRVADAKGDSESEEDEDLEVPVPSR-MKIVDVIGEK-a19-b2	RIIα	RIIα	71	268	0	26.92
HKATEQYYAMK-ILDKQK-a2-b4	Cβ	Cβ	63	76	0.7	26.86
VADAKGDSESEEDEDLEVPVPSR-FPSHFSSDLKDLLR-a5-b10	RIIα	Cβ	71	266	0.88	26.68
KMFESFIESVPLLK-IIVKNNAKK-a1-b8	RIIα	RIIα	246	243	0	26.53
VRFPSHFSSDLKDLLR-KVEAPFIPK-a12-b1	Cβ	Cβ	266	309	0	26.51
AKEDFLR-IVSGKVR-a2-b5	Cβ	Cβ	23	254	0	26.47
LKQIEHTLNEKR-NGVSDIKTHK-a11-b7	Cβ	Cβ	92	292	0	26.44
LKQIEHTLNEK-AKEDFLR-a2-b2	Cβ	Cβ	83	23	0	26.43
VADAKGDSESEEDEDLEVPVPSR-VRFPSHFSSDLKDLLR-a5-b12	RIIα	Cβ	71	266	0	26.3
ATEQYYAMKILDK-LKQIEHTLNEKR-a9-b11	Cβ	Cβ	72	92	0.34	26.27
LEYSFKDNSNLYMVMEYVPGGEMFSHLR-LKQIEHTLNEKR-a6-b11	Cβ	Cβ	111	92	0	26.18
NLLQVDLTKR-AKEDFLR-a9-b2	Cβ	Cβ	279	23	0	26.16
NLLQVDLTKRFGNLK-NGVSDIKTHK-a9-b7	Cβ	Cβ	279	292	0	26.1
IVKADEHVIDQGDDGDNFYVIER-IIVKNNAK-a3-b4	RIIα	RIIα	157	239	0.2	25.73

VADAKGDSESEEDEDLEVPVPSR-MKIVDVIGEK-a5-b2	RIIα	RIIα	71	268	0	25.15
VMLVKHK-ILDKQK-a5-b4	Cβ	Cβ	61	76	0	25.13
DLKPENLLIDHQGYIQVTDFGFAKR-KVEAPFIPK-a24-b1	Cβ	Cβ	189	309	0.37	24.94
IVKADEHVIDQGDDGDNFYVIER-AKEDFLR-a3-b2	RIIα	Cβ	157	23	0	24.77
HKATEQYYAMKILDK-QKVVKLK-a11-b2	Cβ	Cβ	72	78	0.95	24.56
KMFESFIESVPLLK-RIIVKNNAK-a1-b5	RIIα	RIIα	246	239	0.86	24.36
GTYDILVTKDNQTR-LKQIEHTLNEKR-a9-b11	RIIα	Cβ	186	92	0.46	23.96
GTYDILVTKDNQTR-LKQIEHTLNEKR-a9-b2	RIIα	Cβ	186	83	0.52	23.87
LEYSFKDNSNLYMVMEYVPGGEMFSHLR-LKQIEHTLNEKR-a6-b2	Cβ	Cβ	111	83	0.17	23.64
KWENPPPSNAGLEDFER-KVEAPFIPK-a1-b1	Cβ	Cβ	29	309	0	23.61
DLKPENLLIDHQGYIQVTDFGFAKR-AKEDFLRK-a24-b2	Cβ	Cβ	189	23	0	23.48
RKMFESFIESVPLLK-ILDKQK-a2-b4	RIIα	Cβ	246	76	0	23.14
VADAKGDSESEEDEDLEVPVPSRFNR-VRFPSHFSSDLKDLLR-a5-b12	RIIα	Cβ	71	266	0.48	23.09
NISHYEEQLVKMFGSSVDLGNLGQ-VADAKGDSESEEDEDLEVPVPSR-a11-b5	RIIα	RIIα	387	71	0	22.63
VADAKGDSESEEDEDLEVPVPSR-SNKDGGNQEVEIAR-a5-b3	RIIα	RIIα	71	314	0	22.09
ATEQYYAMKILDKQK-LKQIEHTLNEKR-a9-b2	Cβ	Cβ	72	83	0.7	21.98
ILDKQK-NNAKKR-a4-b4	Cβ	RIIα	76	243	0.74	21.72
VADAKGDSESEEDEDLEVPVPSR-KVEAPFIPKFR-a5-b9	RIIα	Cβ	71	317	0	21.64
QSLGHPPPEPGPDRVADAKGDSESEEDEDLEVPVPSR-IVSGKVR-a19-b5	RIIα	Cβ	71	254	0.21	21.59
KMFESFIESVPLLKSLEVSER-RIIVKNNAK-a1-b5	RIIα	RIIα	246	239	0.32	21.46
LKQIEHTLNEKR-AKEDFLR-a11-b2	Cβ	Cβ	92	23	0	21.31
VADAKGDSESEEDEDLEVPVPSR-IVDVIGEKIYKDGER-a5-b8	RIIα	RIIα	71	276	0	21.24
DLKPENLLIDHQGYIQVTDFGFAKR-KKTLGTGSFGR-a24-b2	Cβ	Cβ	189	47	0	21.22
LKQIEHTLNEK-ILDKQKVVK-a2-b4	Cβ	Cβ	83	76	0.95	21.12
KWENPPPSNAGLEDFER-NGVSDIKTHK-a1-b7	Cβ	Cβ	29	292	0.27	20.79
IVKADEHVIDQGDDGDNFYVIER-IYKDGER-a3-b3	RIIα	RIIα	157	279	0.38	20.34
DLKPENLLIDHQGYIQVTDFGFAKR-KKTLGTGSFGR-a24-b1	Cβ	Cβ	189	46	0.23	20.09

Table S5. Quantitative XL-MS comparison of crosslinking site intensity ± AKAP18α. The table lists the relative change in crosslinking between different lysine pairs within RIIβ-Cβ upon inclusion of AKAP18α**.** Lysine pairs are listed starting with the link that was most reduced by inclusion of AKAP18α. Changes in abundance are expressed as $\log_2$ (abundance with AKAP18α/abundance without AKAP18α). *p* value indicates the regression between the two conditions.

Protein A	Protein B	Position A	Position B	$\log_2$-ratio (+18α/-18α)	*p* value
RIIβ	RIIβ	285	324	-2.428	1.32E-09
Cβ	RIIβ	266	46	-1.536	0.0025818
RIIβ	RIIβ	263	46	-1.37	1.58E-05
RIIβ	RIIβ	285	46	-1.237	1.30E-06
RIIβ	RIIβ	357	46	-1.113	0.000116665
Cβ	RIIβ	192	263	-1.096	0.0120618
RIIβ	RIIβ	174	46	-0.655	0.00032057
Cβ	Cβ	192	23	-0.652	1.65E-05
Cβ	RIIβ	81	285	-0.646	0.00159942
RIIβ	RIIβ	326	357	-0.608	0.052444
RIIβ	RIIβ	256	263	-0.547	0.062685
RIIβ	RIIβ	256	285	-0.433	0.00022393
RIIβ	RIIβ	260	263	-0.426	0.042998
RIIβ	RIIβ	260	285	-0.408	0.035763
RIIβ	RIIβ	135	256	-0.39	0.035824
Cβ	Cβ	254	279	-0.362	0.021884
Cβ	Cβ	23	309	-0.332	0.0020576
RIIβ	RIIβ	324	326	-0.316	0.23174
Cβ	RIIβ	254	174	-0.285	0.0066222
Cβ	Cβ	47	61	-0.201	0.35244
RIIβ	RIIβ	174	256	-0.167	0.40362
RIIβ	RIIβ	324	328	-0.145	0.43816
Cβ	Cβ	23	92	-0.033	0.69412
Cβ	Cβ	76	81	-0.029	0.92618
Cβ	Cβ	292	309	0.025	0.86738
Cβ	Cβ	317	47	0.041	0.5802
Cβ	Cβ	292	29	0.068	0.76764
RIIβ	RIIβ	135	285	0.076	0.67778
Cβ	Cβ	317	46	0.105	0.173977
Cβ	Cβ	81	92	0.176	0.130277
Cβ	Cβ	23	292	0.229	0.15416
Cβ	Cβ	23	61	0.251	0.37134
Cβ	Cβ	292	92	0.262	0.37174
Cβ	Cβ	76	92	0.328	0.00040339
Cβ	Cβ	78	83	0.336	0.044683
RIIβ	RIIβ	328	357	0.336	0.000160641

RIIβ	RIIβ	135	174	0.36	0.00058064
Cβ	Cβ	72	92	0.488	0.084118
Cβ	Cβ	29	76	0.558	0.123624
Cβ	Cβ	61	72	0.62	0.048564
Cβ	Cβ	72	81	0.699	0.0199013
Cβ	Cβ	76	83	0.715	4.07E-06
Cβ	Cβ	23	83	0.939	0.00022252
Cβ	Cβ	72	83	0.971	0.011418
Cβ	Cβ	16	292	1.086	1.26E-06